Inorganic Chemistry
Cite This: Inorg. Chem. XXXX, XXX, XXX−XXX
Article
pubs.acs.org/IC

Observation of an Inversion in Photophysical Tuning in a Systematic Study of Luminescent Triazole-Based Osmium(II) Complexes

Paul A. Scattergood,*[†,‡] James Roberts,[†] Salem A. E. Omar,[†] and Paul I. P. Elliott*[†,‡]

[†]Department of Chemistry and [‡]Centre for Functional Materials, University of Huddersfield, Queensgate, Huddersfield HD1 3DH, U.K.

Supporting Information

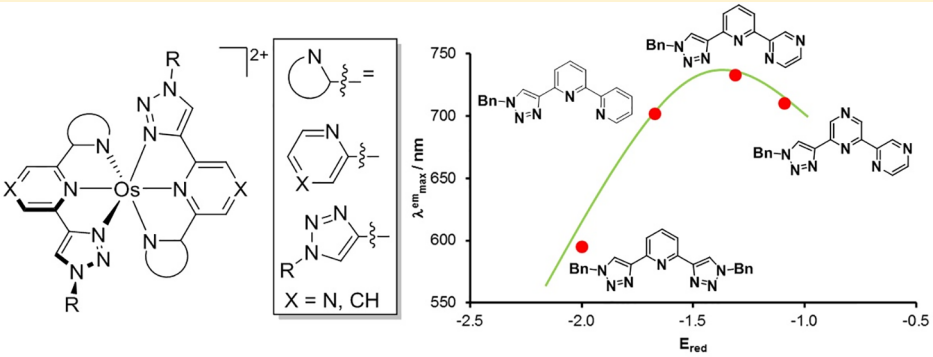

ABSTRACT: In a systematic survey of luminescent bis(terdentate) osmium(II) complexes, a tipping point involving a reversal in photophysical tuning is observed whereby increasing stabilization of the ligand-based lowest unoccupied molecular orbital (LUMO) results in a blue shift in the optical absorption and emission bands. The complexes $[Os(N^N'^N'')_2]^{2+}$ [N^N′^N″ = 2,6-bis(1-phenyl-1,2,3-triazol-4-yl)pyridine (**Os1**), 2,6-bis(1-benzyl-1,2,3-triazol-4-yl)pyrazine (**Os2**), 6-(1-benzyl-1,2,3-triazol-4-yl)-2,2′-bipyridyl (**Os3**), 2-(pyrid-2-yl)-6-(1-benzyl-1,2,3-triazol-4-yl)pyrazine (**Os4**), 2-(pyrazin-2-yl)-6-(1-benzyl-1,2,3-triazol-4-yl)pyridine (**Os5**), and 6-(1-benzyl-1,2,3-triazol-4-yl)-2,2′-bipyrazinyl (**Os6**)] have been prepared and characterized, and all complexes display phosphorescence ranging from the orange to near-IR regions of the spectrum. Replacement of the central pyridine in the ligands of **Os1** by the more π-accepting pyrazine in **Os2** results in a 55 nm red shift in the triplet metal-to-ligand charge-transfer-based emission band, while a larger red shift of 107 nm is observed for the replacement of one of the triazole donors in the ligands of **Os1** by a second pyridine ring in **Os3** (λ^{em}_{max} = 702 nm). Interestingly, replacement of the central pyridine ring in the ligands of **Os3** by pyrazine (**Os4**, λ^{em}_{max} = 702 nm) fails to result in a further red shift in the emission band. Reversal of the relative positions of the pyridine and pyrazine donors in **Os5** (λ^{em}_{max} = 733 nm) compared to **Os4** does indeed result in the expected red shift in the emission with respect to that for **Os3** based on the increased π-acceptor character of the ligands present. However, an inversion in emission tuning is observed for **Os6**, in which the incorporation of a second pyrazine donor in the ligand architecture results in a *blue* shift in the optical absorption and emission maxima (λ^{em}_{max} = 710 nm). Electrochemical studies reveal that while incorporating pyrazine in the ligands indeed results in an expected anodic shift in the first reduction potential through stabilization of the ligand-based LUMO, there is also a concomitant anodic shift in the Os^{II}/Os^{III}-based oxidation potential. This stabilization of the metal-based highest occupied molecular orbital (HOMO) thus nullifies the effect of stabilization of the LUMO in **Os4** compared to **Os3**, resulting in these complexes having coincident emission maxima. For **Os6**, stabilization of the HOMO through the incorporation of two pyrazine donors in the ligand structure now exceeds stabilization of the LUMO, resulting in a larger HOMO−LUMO gap and a counterintuitive blue shift in the optical properties in comparison with those of **Os5**. While it is known that the replacement of ligands (e.g., replacing bipyridyl with bipyrazinyl) can result in a larger HOMO−LUMO energy gap through greater stabilization of the HOMO, these results importantly allow us to capture the tipping point at which this inversion in photophysical tuning occurs. This therefore enables us to explore the limits available in emission tuning with a relatively simple and minimalist ligand structure.

INTRODUCTION

Transition-metal complexes exhibiting phosphorescence in the red/near-IR (NIR) region have been the subject of extensive research.[1] For example, red and NIR emitters have been widely investigated as the phosphor within light-emitting electrochemical cells[2−7] and organic-light-emitting devices,[8−13] including functioning as the low-energy aspect within multi-component white-light systems,[14−18] in addition to finding use as luminescent chemosensors.[19−21] There has also been a notable drive toward the development of complexes that not only display red/NIR emission but also absorb light at longer

Received: March 29, 2019

DOI: 10.1021/acs.inorgchem.9b00915
Inorg. Chem. XXXX, XXX, XXX−XXX

wavelengths. These photophysical characteristics are ideal for achieving effective luminescent cellular imaging agents, where the occurrence of both the absorption and emission of light within the biologically transparent region is highly desirable.[22−25] Further, coordination complexes with electronic absorption profiles extending into the NIR have additionally been identified as necessary in order to improve the efficiency of dye-sensitized solar cells, harvesting photons from an often neglected region of the solar emission spectrum.[26−28]

Over the last few decades, considerable attention has been paid to coordination complexes of kinetically inert d^6 metals such as rhenium(I), ruthenium(II), iridium(III), and osmium(II).[29] The photophysical properties of these complexes are well understood and documented, with the excited state frequently dominated by long-lived triplet metal-to-ligand charge-transfer (^{3}MLCT) states from which phosphorescence occurs and from where further electron-transfer events are possible. With a view toward achieving low-energy photoluminescence and potential applications in luminescence cellular imaging, complexes of osmium(II) offer several advantageous photophysical properties. First, the high spin−orbit coupling constant associated with the heavy-metal center gives rise to formally spin-forbidden ground state-to-^{3}MLCT state electronic absorption bands of appreciable extinction coefficient, which occur at significantly lower energy than the corresponding spin-allowed transitions which populate the singlet metal-to-ligand charge-transfer (^{1}MLCT) states.[30] Further, these excitation bands are typically red-shifted compared with those observed for comparable complexes of the group 8 congener ruthenium(II), with photoluminescence from osmium(II) complexes occurring in the deep-red-to-NIR spectral region. For example, bis(terdentate) complexes of osmium(II) featuring 6-[5-(trifluoromethyl)pyrazol-3-yl]-2,2′-bipyridine ligands have previously been reported to display appreciable panchromatic electronic absorption profiles and low-energy luminescence with λ_{em} = 655−935 nm.[31] These properties are ideal for potential cellular imaging agents, enabling a greater depth of tissue penetration for excitation, reducing biological damage through the use of lower-energy excitation sources, and avoiding autofluorescence from chromophores within the biological material.

While complexes of d^6 metals, particular those of ruthenium(II) and iridium(III), have been extensively developed for luminescence biological imaging applications, the use of osmium(II) complexes for this purpose is rather rare. Keyes and co-workers[32] have reported an osmium(II) polypyridyl−polyargenine conjugate for live cell imaging, while Chao and co-workers[33] have investigated a benzimidazolylpyridine-containing osmium(II) complex as a lysosomal tracker that displays deep-red emission with λ_{em} = 736 nm. Very recently, Zhang and co-workers[34] have reported emissive osmium(II) polypyridyl complexes featuring iminopyridine ligands that permit NIR luminescence imaging of RNA and nucleoli of live cells. Our own group has previously investigated 1,2,3-triazole-based complexes of osmium(II), with complexes in the series $[Os(bpy)_{3-n}(pytz)_n]^{2+}$ [bpy = 2,2′-bipyridyl; pytz = 1-benzyl-4-(pyrid-2-yl)-1,2,3-triazole; n = 0−3] displaying phosphorescence within the deep-red spectral region.[35] The homoleptic species $[Os(pytz)_3]^{2+}$ was found to result in the luminescent staining of lysosomes and endosomes within two cancer cell lines. In a related study, we have also prepared the osmium(II) complex $[Os(btzpy)_2]^{2+}$ of the terdentate ligand 2,6-bis(1-phenyl-1,2,3-triazol-4-yl)pyridine (btzpy), which displays emission at 595 nm and preferentially localizes within the mitochondria of HeLa and U2OS cell lines, allowing for luminescence imaging by confocal microscopy.[36] These initial studies also revealed that the homoleptic triazole-containing complexes exhibited significant luminescence quenching in the presence of oxygen, with the sensitization of singlet oxygen thus providing the basis for the development of potential dual-mode photodynamic theranostic agents.

While offering promise, the absorption and emission bands exhibited by the complexes in our initial investigations were not ideally situated in the optical spectrum so as to optimally align with the biologically transparent window. To expand upon our previous studies, we were motivated to design and develop new terdentate ligand architectures in order to shift the absorption and emission characteristics of the resultant osmium(II) complexes firmly into the deep-red/NIR region. Because of the synthetic versatility of the 1,2,3-triazole motif for ligand design, the aforementioned singlet-oxygen-sensitizing activity, and also the reported facile conjugation of complexes to biologically relevant targeting moieties[37] through 1,2,3-triazole-based linkers, we were minded to retain this heterocycle in our ligands appearing in the systematic survey reported here. In order to maintain a relatively simple ligand architecture for reasons of facile synthetic accessibility and concerns over resultant complex solubility, these triazole donors were therefore combined in both symmetric and asymmetric terdentate ligands with more electron-withdrawing pyridine and pyrazine donor rings. Through this approach we were confident in achieving a lowering of the energy of the ligand-based lowest unoccupied molecular orbital (LUMO) and thus a red shift of the optical absorption and emission bands of the complexes.

While the parent terdentate ligand 2,2′:6′,2″-terpyridine (tpy) is ubiquitous in the coordination chemistry of photoactive metal complexes, we note that derivatives and analogues often carry peripheral substituents, primarily upon the pyridyl rings, with the core of the ligand framework remaining intact.[38] Less attention has been paid to the synthesis and development of unsubstituted tpy analogues containing higher azines or alternative N-donor heterocycles. Pyrazine-based ligands in complexes of osmium(II) are relatively rare in the literature but have been reported, for example, in investigations of electron transfer and delocalization,[39] in addition to being featured within higher-chelating-ligand structures, facilitating coordination to two metal centers and thus the formation of bi- and multimetallic systems.[40] The group of Brewer has extensively explored use of the 2,3-bis(2-pyridylpyrazine) ligand,[41,42] including in osmium(II)-containing multimetallic systems displaying NIR absorption,[43] while Campagna and co-workers have utilized the same framework and derivatives thereof in the synthesis of multimetallic dendrimers, which function as light-harvesting antenna.[44] While the use of pyrazine as a bridging ligand is more widespread, its employment within polyazine ligands of monometallic complexes is relatively sparse. For example, Ruminski and co-workers have investigated a homoleptic osmium(II) complex of dipyrido-2,3-*a*;3′,2′-*j*-phenazine ($[Os(dpop')_2]^{2+}$), which has an UV−visible absorption profile extending to ∼800 nm and displays weak phosphorescence with λ_{em} = 795 nm.[45]

In this contribution, we explore the design and synthesis of new symmetrical and asymmetrical terdentate ligand architectures featuring pyridine, pyrazine, and 1,2,3-triazole donor moieties and investigate their coordination chemistry with

DOI: 10.1021/acs.inorgchem.9b00915
Inorg. Chem. XXXX, XXX, XXX−XXX

Scheme 1. Synthetic Route to Terdentate Ligands 1 and 3

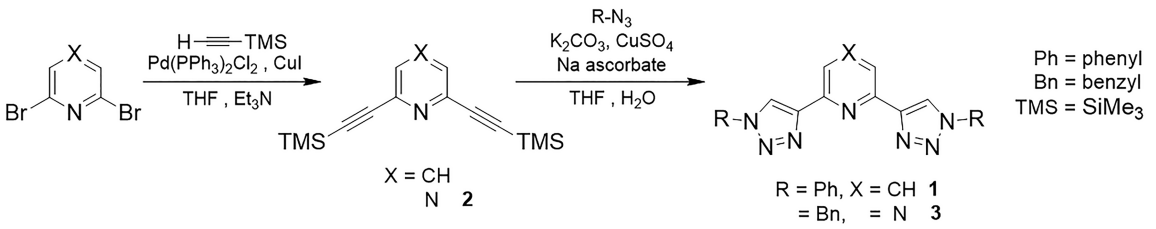

Scheme 2. Synthetic Route to Terdentate Ligands 7 and 10

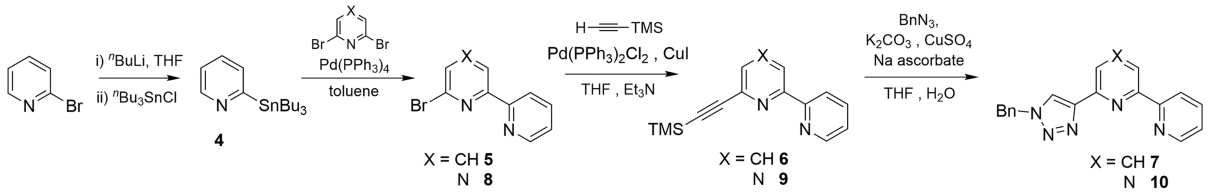

Scheme 3. Synthesis of the Terdentate Ligands 14, 17, and 18

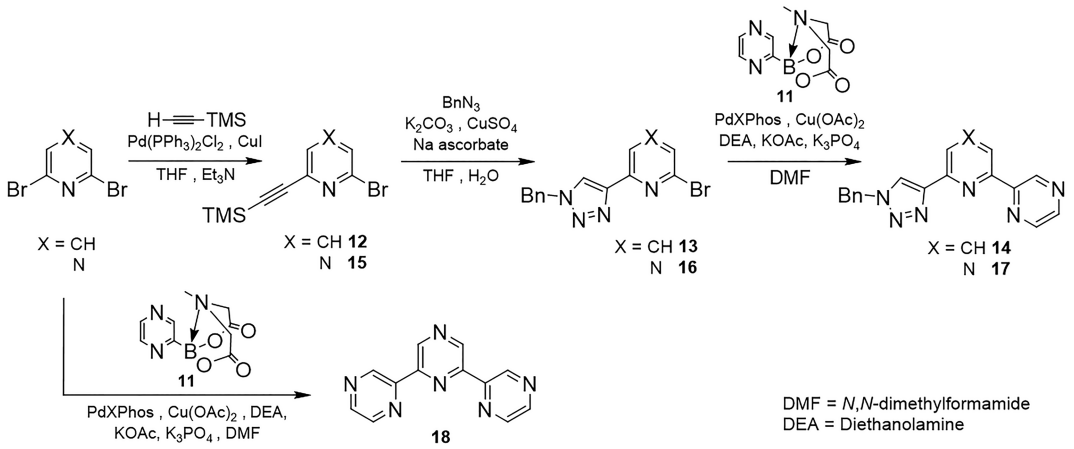

osmium(II). These bis(terdenate) complexes are emissive in the red/NIR region, with not only the identity but the specific positioning of the azines within the ligand framework having a significant effect upon the photophysical and electrochemical properties of the complexes as a whole. Further, we show that while the expected increase in the electron-withdrawing character does indeed stabilize the LUMO of the complexes, the incorporation of pyrazine donors also has a significant stabilizing effect on the predominantly Os d-orbital-based highest occupied molecular orbital (HOMO). Thus, we observe a tipping point in our series where stabilization of the HOMO outweighs stabilization of the LUMO and the trend in photophysical tuning becomes inverted.

■ RESULTS AND DISCUSSION

In a fashion similar to that of the previously reported synthesis of **1**,[46,47] the pyrazine-containing ligand 2,6-bis(1-benzyl-1,2,3-triazol-4-yl)pyrazine (**3**) was conveniently prepared through the copper-catalyzed alkyne−azide cycloaddition (CuAAC) of 2,6-bis(ethynyltrimethylsilyl)pyrazine (**2**) and benzyl azide (Scheme 1). The ^{1}H NMR spectrum of **3** is simple, with singlets at δ 8.05 and 9.30 corresponding to the triazole ring and equivalent pyrazinyl protons, respectively. The methylene protons of the benzyl substituents are observed as a further singlet at δ 5.59, while the benzylic aromatic protons fall within the multiplets at δ 7.26−7.43.

The 1,2,3-triazole-appended 2,2′-bipyridyl ligand **7** was prepared via a four-step procedure starting from 2-bromopyridine (Scheme 2). Briefly, palladium-catalyzed Stille cross-coupling of the stannane **4** with a stoichiometric quantity of 2,6-dibromopyridine afforded 6-bromo-2,2′-bipyridyl (**5**), which subsequently underwent palladium-catalyzed Sonogashira cross-coupling with ethynyltrimethylsilane to give the corresponding ethynyl-substituted bipyridine **6**. A further CuAAC reaction with benzyl azide furnished the desired ligand **7** with a modest yield of 44%. We were additionally able to introduce a pyrazine heterocycle into the terdentate ligand structure (**10**) by following an analogous synthetic route utilizing 2,6-dibromopyrazine (Scheme 2). ^{1}H NMR spectra of the ligands **7** and **10** feature the characteristic singlet triazole ring resonances at δ 8.17 and 8.18, respectively. The placement of the pyrazine ring in the central position of the tris-heterocycle ligand **10** leads to a loss of symmetry for the pyrazine moiety, resulting in the observation of two downfield singlet resonances in the ^{1}H NMR spectrum at δ 9.43 and 9.54 attributed to the 3 and 5 positions, respectively, assigned through nuclear Overhauser effect (NOE) correlation data.

In order to determine the effect of the relative positions of the pyridine and pyrazine donors on the photophysical

DOI: 10.1021/acs.inorgchem.9b00915
Inorg. Chem. XXXX, XXX, XXX−XXX

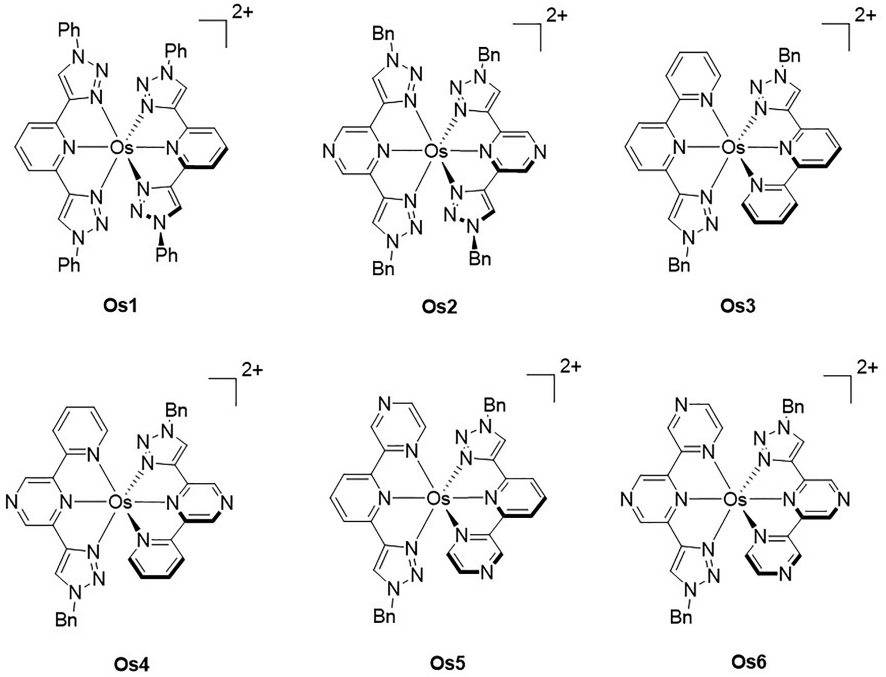

Figure 1. Structures of the osmium(II) complexes investigated in this work.

properties of subsequent complexes, we targeted ligand **14** featuring a central pyridine and peripheral pyrazine rings (Scheme 3). An obvious synthetic strategy would be one directly analogous to that described above, employing a stannylpyrazine reagent. However, despite reports concerning the preparation of 2-(tributylstannyl)pyrazine,[48,49] we were unable to successfully isolate this species in any appreciable yield. These difficulties, in addition to the inherent toxicity of tin reagents and problems frequently encountered during the purification of Stille cross-coupling products, led us to seek an alternative synthetic solution. Burke and co-workers have recently reported the robust preparation of a range of 2-heterocyclic *N*-methyliminodiacetic acid (MIDA) boronates, suitable as coupling partners in palladium-catalyzed cross-coupling reactions.[50] While 2-heterocyclic boronic acids are generally unstable and difficult to handle, MIDA boronates are found to be both air- and moisture-stable and are readily prepared. These reagents have additionally been trialled within Suzuki-type reactions, where they have proven to be effective in providing the in situ "slow release" of unstable but reactive boronic acids, thereby functioning as effective building blocks in the synthesis of a range of heterocyclic organic frameworks.[51]

The 2-pyrazinyl MIDA boronate (**11**) was prepared via the reported procedure[50] and obtained with a yield of 53%. Initial attempts to cross-couple **11** with a stoichiometric quantity of 2,6-dibromopyrazine gave predominantly the bis-substituted product. Consequently, the 1,2,3-triazole moiety was appended first via 2-bromo-6-ethynylpyridine and a subsequent CuAAC reaction with benzyl azide to produce **13** (Scheme 3). Further reaction with pyrazine MIDA boronate **11** was carried out following a two-pot procedure, successfully furnishing the target ligand **14** with a modest yield of 45%.

We were additionally able to apply this synthetic methodology and the use of a pyrazinyl MIDA boronate to produce the triazole−bipyrazine ligand **17** (Scheme 3). The triazole ring proton of **17** is readily observed in the ^{1}H NMR spectrum as a singlet at δ 8.91, assigned through a strong NOE correlation with the methylene protons of the benzyl group, themselves giving rise to a singlet at δ 5.79. COSY spectra allow the protons on the 5 and 6 positions of the peripheral pyrazine ring to be identified as a pair of strongly coupled resonances at δ 9.62 and 8.72, with the proton on the 3 position, together with those of the central pyrazine ring appearing as three singlet resonances at δ 9.44, 9.37, and 8.74. The lack of coupling interactions and absence of obvious correlation signals in NOESY NMR spectra preclude the specific assignment of these resonances.

Finally, **11** was utilized further to access the tris-pyrazinyl ligand **18** (Scheme 3). Surprisingly, only two reports have previously been made concerning the synthesis of this polyaza species,[38,49] both of which rely on the Stille coupling of a stannylpyrazine with chloropyrazines. Here, employment of the Suzuki coupling of **11** with 2,6-dibromopyrazine gives **18** with a moderate yield of 28%.

The osmium(II) complexes of the reported terdentate ligands (**Os1**−**Os6**; Figure 1) were all conveniently prepared as their hexafluorophosphate salts by the reaction of 1 equiv of the appropriate ligand with $[OsCl_6][NH_4]_2$ in refluxing ethylene glycol followed by treatment with NH_4PF_6. Purification by either column chromatography or recrystallization gave the bis(terdentate) complexes as brown-to-dark-green powders. ^{1}H NMR analysis of the complexes gave spectra similar to those of the free ligands, although with protons on the coordinating fragments being marginally deshielded. For example, the triazole ring and pyrazinyl protons of ligand **3** are observed at δ 8.37 and 9.18, respectively, in deuterated acetonitrile (MeCN-d_3), while the corresponding resonances for **Os2** appear at δ 8.66 and 9.28. Attempts were also made to prepare the bis(terdentate) osmium(II) complex of 2,2′:6′,2″-terpyrazine (**Os7**) both in an analogous manner to **Os1**−**Os6** and via an alternative route involving the reaction between $[\{Os(C_6H_6)Cl_2\}_2]$ and 4 equiv of ligand **18** in refluxing ethanol (EtOH)/water (H_2O). All

DOI: 10.1021/acs.inorgchem.9b00915
Inorg. Chem. XXXX, XXX, XXX−XXX

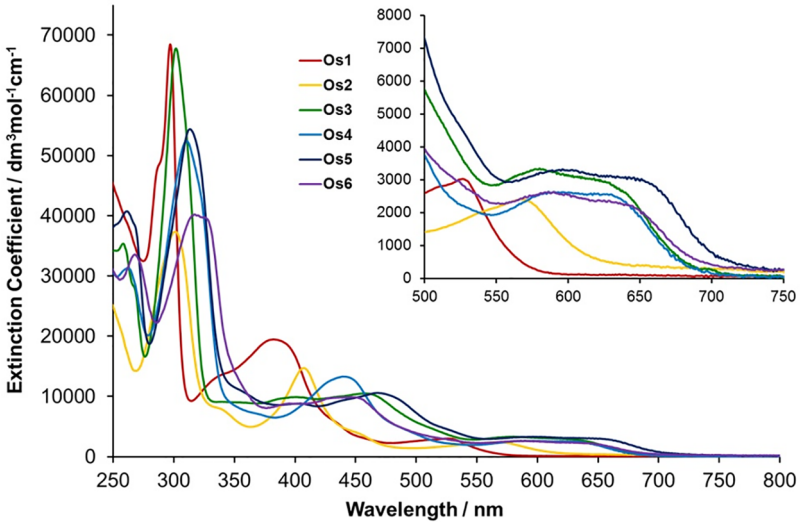

Figure 2. UV−visible electronic absorption spectra recorded for MeCN solutions of **Os1**−**Os6** (inset: magnification of the region containing bands for direct singlet ground state to ^{3}MLCT state transitions).

Table 1. Summarised Photophysical Data for Os1−Os6

	λ_{abs}[a]/nm (ε/dm^3 mol^{-1} cm^{-1})	λ_{em}[a]/nm (RT)	Φ_{em}[a,b]/% (air)	Φ_{em}[b,c]/% (degassed)	τ_{em}[a]/ns (air)	τ_{em}[c]/ns (degassed)	λ_{em}[d]/nm (77 K)
Os1	530 (2960), 436 (5570), 385 (19400), 338 (13550), 297 (68475), 288 (48600), 242 (49000)	595[e]	0.8	9.3	63	937	564, 606 (sh)
Os2	570 (2400), 452 (3900), 409 (14550), 339 (7900), 302 (37300), 248 (25800), 229 (33260)	650[f]	1.1	3.5	269	924	625, 673 (sh)
Os3	631 (2830), 581 (3320), 462 (10450), 400 (9900), 302 (67550), 268 (27775), 259 (34930)	702[g]	1.0	2.9	88	253	676, 741 (sh)
Os4	633 (2480), 587 (2620), 493 (4330), 442 (13280), 312 (52125), 265 (30650), 243 (33970)	702[g]	1.2	2.5	155	240	687, 746 (sh)
Os5	656 (2910), 596 (3320), 523 (4735), 471 (10500), 441 (9430), 405 (8850), 358 (10675), 315 (54075), 263 (40435)	733[g]	1.1	1.8	135	216	703, 769 (sh)
Os6	641 (2230), 590 (2620), 452 (9780), 430 (9750), 396 (8830), 328 (39370), 319 (40025), 269 (33380), 243 (33000)	710[g]	1.7	2.9	186	288	690, 752 (sh)

[a]Aerated MeCN. [b]Relative to $[Ru(bpy)_3][PF_6]_2$, Φ_{em} = 0.018 in aerated MeCN.[53] [c]Degassed MeCN. [d]4:1 EtOH/MeOH. [e]λ_{ex} = 500 nm. [f]λ_{ex} = 550 nm. [g]λ_{ex} = 580 nm.

synthetic attempts resulted in the production of a very dark-green intractable powder, which remained highly insoluble after metathesis with NH_4PF_6 and $NH_4BAr^F{}_4$ salts. Indeed, very poor solubility has been encountered previously in complexes of this terpyrazine ligand.[38] We have thus been unable to confirm the successful synthesis of **Os7** and so discount it from further experimental discussions.

UV−visible electronic absorption spectra were recorded for MeCN solutions of **Os1**−**Os6** and are shown in Figure 2, with summarized spectroscopic data presented in Table 1. The spectrum of **Os2** exhibits an intense absorbance at 302 nm, which is assigned to a $\pi \rightarrow \pi^*$ transition localized on the ligand (**3**), shifted to lower energy compared to a similar ligand-based transition observed for the previously reported complex **Os1** (297 nm).[36] **Os2** displays further electronic absorbance features within the visible region, with those between 370 and 450 nm assigned to ^{1}MLCT transitions and weaker bands at 520−630 nm attributed to the direct population of ^{3}MLCT states, an electronic absorbance feature characteristic of osmium(II) polypyridyl type complexes as a consequence of the high spin−orbit coupling constant of the metal center.[30,52] The ^{1,3}MLCT bands observed for **Os2** are shifted to lower energy compared to those of **Os1**, indicative of a lower-energy LUMO as the pyridine moiety is replaced with the more π-accepting pyrazine.

Electronic absorption spectra of **Os3**−**Os6** are panchromatic, displaying intense absorbance bands in the UV region in addition to strong bands within the visible region, which tail-off at ∼700 nm. For **Os3**, an intense band centered at 302 nm is assigned to $\pi \rightarrow \pi^*$ intraligand transitions, while the ^{1}MLCT and ^{3}MLCT absorption envelopes are observed within the regions 400−500 and 550−680 nm, respectively. These charge-transfer bands are stabilized in energy with respect to **Os1**−**Os2**, primarily as a consequence of the partial replacement of 1,2,3-triazole moieties with pyridyl units and subsequent stabilization of the ligand-based LUMO. The incorporation of more efficient π-accepting units in the form of pyrazine into the ligand set of complex **Os4** may be reasonably expected to further stabilize the ^{1,3}MLCT states. However, when the absorbance profile of **Os4** is compared to that of **Os3**, the positions of the charge-transfer bands appear to be unchanged. Moving from **Os4** to **Os5**, where the positions of the pyridyl and pyrazinyl units within the ligands are exchanged, it is likely that the LUMO remains mostly pyrazine-based and as such is now positioned much further away from the 1,2,3-triazole unit, which has an appreciable destabilizing influence as a consequence of its poor π-acceptor

DOI: 10.1021/acs.inorgchem.9b00915
Inorg. Chem. XXXX, XXX, XXX−XXX

ability. This therefore might be expected to lead to a reduction in the energy of the LUMO for **Os5** over that of **Os4**. Indeed, in agreement with this reasoning, the ^{1,3}MLCT bands of **Os5** appear at lower energy with respect to those of **Os4**, with the ^{1}MLCT maximum recorded at 471 nm and the ^{3}MLCT absorbance tailing off beyond 720 nm. While **Os6** with its bis(pyrazinyl)-containing ligands may be reasonably expected to give further stability to charge-transfer transitions, it is interesting to note that the ^{1,3}MLCT bands are of a similar spectral position to those recorded for **Os3** and **Os4** and are, in fact, *blue-shifted* relative to those of **Os5**.

Complexes **Os1**−**Os6** were found to be emissive in aerated MeCN solutions from the orange to deep-red/NIR spectral regions (Figure 3 and Table 1), with broad, featureless bands

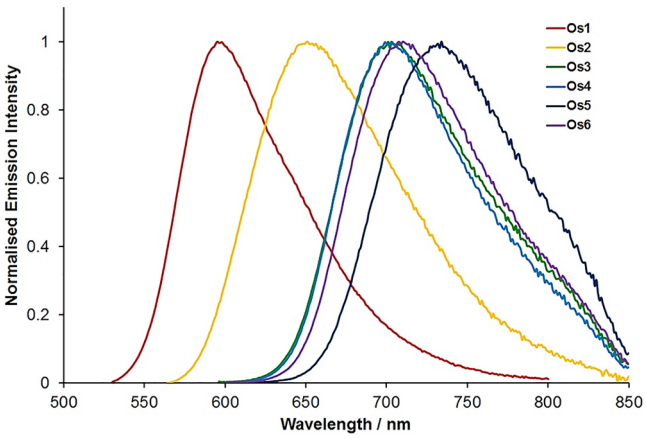

Figure 3. Normalized corrected emission spectra recorded for aerated MeCN solutions of **Os1**−**Os6** at RT.

suggesting that the luminescence originates from states having predominantly ^{3}MLCT character. It is pertinent to note that the emissive ^{3}MLCT state in **Os3**−**Os6** can be accessed through direct excitation into the spin-forbidden ^{3}MLCT absorption band at wavelengths ≥600 nm, ideal for biological imaging applications, for example, where excitation within the biological transparent region is highly desirable. The emission intensity is affected by the presence of oxygen in all cases; however, the level of quenching in aerated solutions compared to degassed solutions generally diminishes as the emission bands become progressively more red-shifted and the lifetime of the excited state becomes shorter. **Os2** exhibits an emission maximum at 650 nm, shifted by some 1420 cm^{-1} (55 nm) to lower energy than **Os1** as a result of replacement of the central pyridyl moiety with pyrazine and subsequent stabilization of the ^{3}MLCT state. This observation is in agreement with UV−visible electronic absorption data (vide supra) and the expectation of a significantly stabilized ligand-based LUMO. Emission bands for **Os3**−**Os6** are red-shifted still further, with emission maxima beyond 700 nm placing the observed phosphorescence within the NIR region. In accordance with their electronic absorption spectra, **Os3** and **Os4** have identically positioned emission maxima (λ_{em} = 702 nm), whereas the lower-lying ^{3}MLCT state in **Os5** results in a lower-energy emission with a maximum at 733 nm. It is noteworthy that the specific placement of the three heterocycles within the isomeric terdentate ligands of **Os4** and **Os5** has an appreciable influence on the photophysical properties, with a flanking pyrazine moiety evidently resulting in a more stabilized LUMO. Mirroring the unexpectedly blue-shifted charge-transfer absorption bands recorded for **Os6** relative to those of **Os5**, emission from **Os6** is noted at 710 nm. These observations clearly indicate that the ^{3}MLCT state of **Os5** is stabilized over that of **Os6**, despite the ligand-localized LUMO of the latter likely to be lower-lying by virtue of the inclusion of four π-accepting pyrazinyl units. We also note that while the emission quantum yield for the lowest-energy emitter (**Os5**) is small (∼1%), it remains comparable to both the other complexes within this series and previously reported osmium(II) polypyridyl complexes, particularly those that emit in the deep-red/NIR region,[31] which are known to be weak emitters at room temperature (RT).[7,30,35]

Photoluminescence lifetimes were recorded for all complexes **Os1**−**Os6** in both aerated and degassed MeCN solutions (Table 1). The emission lifetime for each complex was found to be elongated in the absence of oxygen, indicating the occurrence of luminescence from an excited state of triplet

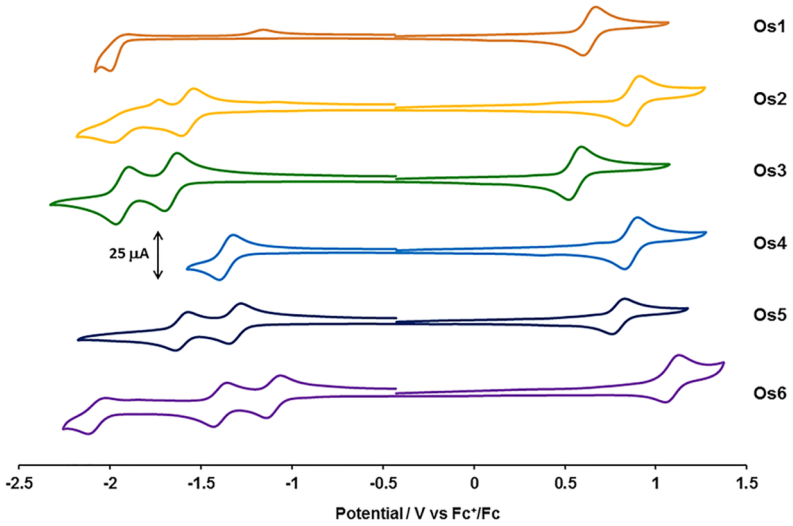

Figure 4. Cyclic voltammograms for 1.5 mmol dm^{-3} MeCN solutions of complexes **Os1**−**Os6** recorded at RT at 100 mV s^{-1}. Solutions contained 0.2 mol dm^{-3} NBu_4PF_6 as the supporting electrolyte. All potentials are shown against the Fc^+/Fc couple.

DOI: 10.1021/acs.inorgchem.9b00915
Inorg. Chem. XXXX, XXX, XXX−XXX

Table 2. Summarized Electrochemical Data for 1.5 mmol dm^{-3} MeCN Solutions of Complexes Os1−Os6 Measured at RT at a Scan Rate of 100 mV s^{-1}[a]

complex	E_{ox}/V	E_{red}/V	(E_{ox} − E_{red})/V
Os1	+0.64 (67)	−2.00[b]	2.64
Os2	+0.88 (77)	−1.58 (61), −1.99[b]	2.46
Os3	+0.56 (72)	−1.67 (67), −1.93 (72)	2.23
Os4	+0.87 (77)	−1.36 (76), −1.72[b,c]	2.23
Os5	+0.80 (76)	−1.31 (66), −1.61 (66)	2.11
Os6	+1.09 (68)	−1.09 (77), −1.39 (69), −2.07 (83)	2.18

[a]Potentials are shown in V vs Fc^+/Fc. Anodic−cathodic peak separations ($\Delta E_{a,c}$) for reversible couples are shown in mV within parentheses ($\Delta E_{a,c}$ for Fc^+/Fc was typically 70 mV). [b]Cathodic peak potential. [c]Process not shown in Figure 4; see Figure S32.

character and confirming our assignment to phosphorescence from a ^{3}MLCT state. Indeed, we have previously found that **Os1** is an efficient sensitizer of singlet oxygen [$\Phi(^1O_2)$ = 57%] with the intensity of phosphorescence undergoing a 43-fold reduction between degassed and oxygenated MeCN solutions.[36] Further inspection of the degassed photoluminescence lifetimes for **Os1−Os6** reveals a close agreement with the energy gap law.[54,55] Complex **Os1** displays the highest emission energy and correspondingly the longest lifetime of 937 ns, which is seen to shorten across the series as the emission energy decreases. The lowest-energy emitter, **Os5**, displays the shortest lifetime of 135 ns, marginally shorter than that of **Os6**, where the emission maximum is shifted to slightly shorter wavelength (Figure 3). Photoluminescence quantum yields for degassed solutions are also found to mirror this trend, again in good agreement with the energy gap law, with **Os1** being the most efficient emitter within the series (Φ = 9.3%), decreasing systematically with the steady reduction in energy of photoluminescence to **Os5** (Φ = 1.8%).

Low-temperature emission spectra were recorded for **Os1−Os6** at 77 K in EtOH/methanol (MeOH) glass mixtures (Figure S31). The emission profiles reveal additional vibronic structure, with maxima shifted to higher energy relative to the solution-state spectra as a result of rigidochromic effects. While the emission profiles of **Os3** and **Os4** are now separated, with maxima at 676 and 687 nm, respectively, the general trend in the emission energy across the series remains unchanged in frozen solvent glass, with **Os5** still exhibiting the lowest-energy emission with a maximum at 703 nm.

Cyclic voltammograms recorded for complexes **Os1−Os6** are shown in Figure 4 with summarized electrochemical data presented in Table 2. At least one reduction process is observed for each complex **Os1−Os6** within the available electrochemical solvent window, all of which are assigned to ligand-based processes. The trend in the potential of the reductive electrochemistry is generally in agreement with our initial expectations. Replacement of the central pyridine in the ligands of **Os1** by pyrazine in the ligands of **Os2** results in an anodic shift of 0.42 V. The first reductions for **Os4** and **Os5** appear at more positive potential than that of **Os3** because of stabilization of the ligand-based LUMO, again owing to the incorporation of pyrazine donors within the ligand structure. In agreement with earlier interpretations based on spectroscopic data, it is noted that the positioning of the pyrazine moiety in a flanking rather than central position within the ligand structure results in enhanced stabilization of the LUMO, with the first reduction of **Os5** appearing at a slightly more positive potential than that of **Os4**. The presence of two π-accepting pyrazine moieties within each ligand of **Os6** results in the appearance of the most anodically shifted first reduction potential at −1.09 V, in line with the assumption that this ligand results in the most stabilized LUMO of all complexes within the series.

All complexes exhibit a reversible oxidation process, which is assigned to the Os^{II}/Os^{III} couple. On the basis of our previous work, together with that of others, we initially expected the potential of this oxidation process, although perturbed, to be relatively insensitive to the changing nature of the ligands across the series owing to the HOMO being predominantly Os d orbital in character.[7,12,35,56,57] However, the electrochemical data reveal this couple to also be significantly affected by the incorporation of pyrazine units within the ligand set, with the first oxidation potentials for **Os2**, **Os4**, and **Os5** appearing within the region +0.80−0.88 V versus ferrocene/ferrocenium (Fc^+/Fc), shifted anodically by ca. 0.25 V compared to those of **Os1** and **Os3**. The use of bis(pyrazinyl)-containing ligands within complex **Os6** results in an even greater positive shift in the first oxidation potential, appearing at +1.09 V.

It is therefore evident that, unlike in our previous studies where the relative energy of the ligand-based LUMO broadly dictates the overall observed changes and trends in the photophysical properties of the complexes, for this series, the significant variance in the energy of the HOMO makes a key contribution to the spectroscopic properties. The introduction of one pyrazine ring into the terdentate ligand architectures generally leads to stabilization and a red shift in the absorption and emission bands, but the extent of this tuning is undermined by concomitant stabilization of the HOMO with that of the LUMO. For **Os4**, the spectroscopic changes by virtue of stabilization of the LUMO with respect to that of **Os3** through the replacement of a pyridine by pyrazine are canceled out by stabilization of an almost equal magnitude of the HOMO. When two pyrazine rings are incorporated in each ligand in **Os6**, additional stabilization observed for the HOMO outweighs stabilization of the LUMO, resulting in an increased HOMO−LUMO gap. Thus, the trend in the HOMO−LUMO energy gap revealed through electrochemistry perfectly matches those trends observed in the electronic absorption and luminescence spectra (vide supra) and explains the reversal in MLCT energy tuning observed upon going from **Os5** to **Os6**.

Upon examination of the literature, we note that these results on pyrazine ligand-based stabilization of the HOMO are in agreement with previously reported data on ruthenium(II) and osmium(II) complexes. While the first reduction potential for $[Ru(bpz)_3]^{2+}$ (bpz = 2,2′-bipyrazine) appears 0.63 V to more positive potential than that for $[Ru(bpy)_3]^{2+}$, the Ru^{II}/Ru^{III} oxidation of the former is anodically shifted to a greater degree (0.71 V),[58] resulting in a blue shift in both ^{1}MLCT absorptions and the ^{3}MLCT-based emission band (from 609 nm for $[Ru(bpy)_3]^{2+}$ to 600 nm for $[Ru(bpz)_3]^{2+}$ in

DOI: 10.1021/acs.inorgchem.9b00915
Inorg. Chem. XXXX, XXX, XXX−XXX

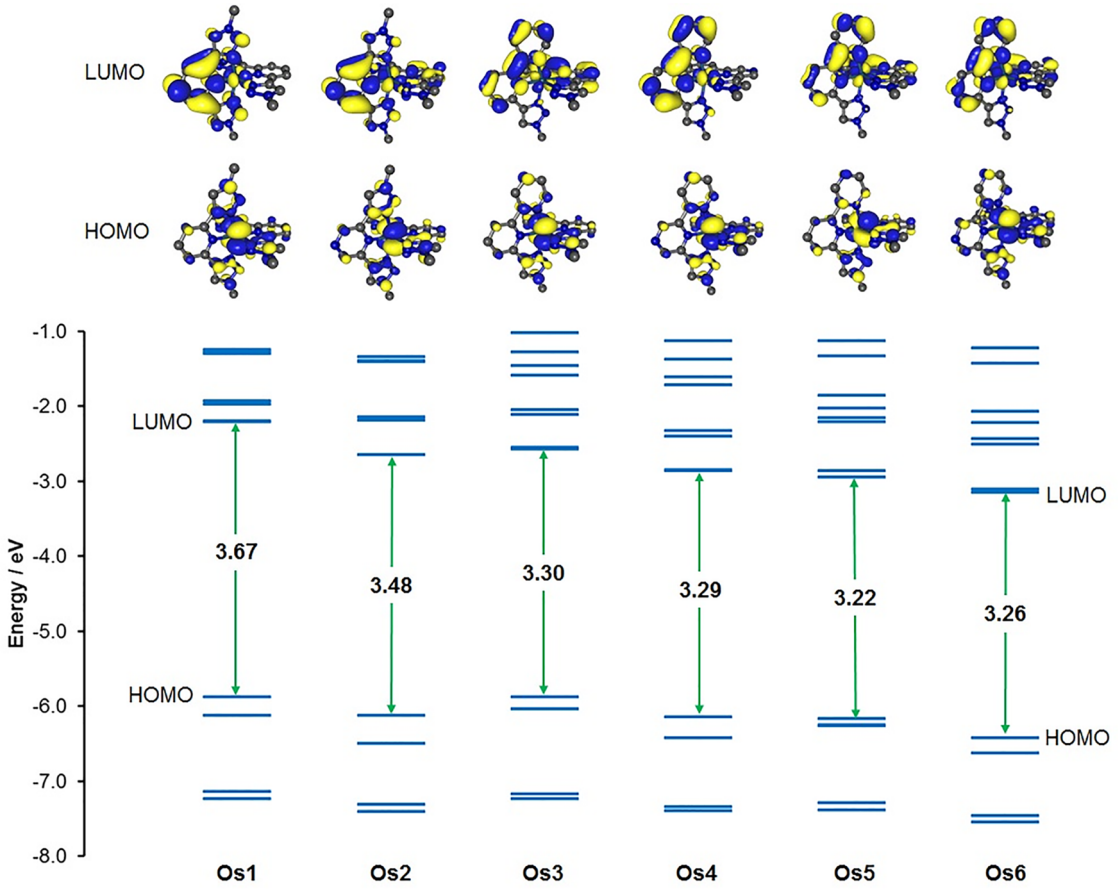

Figure 5. Molecular orbital energy-level diagram for complexes **Os1**−**Os6** and plots of the HOMOs and LUMOs in each case.

H_2O).[59] An analogous blue shift in emission is observed for $[Os(bpz)_3]^{2+}$ (700 nm in MeCN) compared to $[Os(bpy)_3]^{2+}$ (724 nm), where the oxidation potential of the former is anodically shifted by 0.70 V with respect to that of the latter, while the first reduction potential of $[Os(bpz)_3]^{2+}$ is positively shifted by 0.59 V.[60]

To complement and corroborate our experimental spectroscopic and electrochemical studies, we carried out density functional theory (DFT) calculations to determine the nature of the frontier orbitals and the influence of the ligands on their relative energies. The calculated relative energies of the HOMO and LUMO for the series of complexes (Figure 5) are in excellent agreement with the experimental electrochemical data (vide supra). Replacement of the central pyridine in the ligands in **Os1** by pyrazine as in **Os2** results in stabilization of the LUMO by 0.44 eV, with a concomitant lesser stabilization of the HOMO leading to a reduction in the HOMO−LUMO gap by 0.2 eV. The larger π system associated with the triazolylbipyridine ligands in **Os3** results in a stabilization of the LUMO comparable to that for **Os2** with respect to **Os1**. The results confirm the electrochemical data, which show that the red shift in the optical absorption and emission profiles for **Os3** derives from the HOMO undergoing little or no modulation in energy by virtue of the number of triazole donors in the ligand set in comparison with **Os1**.

The replacement of either the central or outer pyridine ring by pyrazine in the ligands in **Os4** and **Os5** again leads to stabilization of the HOMO as well as the LUMO. The HOMO and LUMO in **Os4**, incorporating the pyrazine as the central donor in the terdentate ligands, are each stabilized to the same extent in comparison to the frontier orbitals of **Os3**, leading to an almost identical HOMO−LUMO energy gap. This is in agreement with the electrochemical data, the resultant and unexpected lack of a red shift in the optical absorption spectrum, and a coincident emission maximum for this complex compared to **Os3**. Placement of the pyrazine as the outer ring of the terdentate ligands in **Os5** leads to a comparable energy of the HOMO with respect to that of **Os4**, but removal of the destabilizing influence of a neighboring triazole moiety results in stabilization of the LUMO by a further 0.1 eV. This is again in agreement with the electrochemical data and experimentally observed red shift in the absorption and emission profiles of **Os5** compared to those of **Os4**.

While the replacement of both pyridine donors in the ligands for **Os3** with pyrazine in the ligands for **Os6** leads to significant stabilization of the LUMO, this also leads to greater stabilization of the HOMO, resulting in an enlargement of the HOMO−LUMO gap compared to **Os5**. The calculated data are therefore in agreement with the experimental electrochemical data, confirming the observed inverted tuning of the ^{1}MLCT and ^{3}MLCT energies through an increase in the number of π-accepting pyrazine moieties in the ligand architecture.

While we were not able to synthetically isolate the terpyrazine (tpz) complex $[Os(tpz)_2]^{2+}$ (**Os7**), we might predict that it would possess absorption and emission spectra further blue-shifted compared to those of **Os6** based on the experimental data for bpz complexes compared to those of

DOI: 10.1021/acs.inorgchem.9b00915
Inorg. Chem. XXXX, XXX, XXX−XXX

their bpy analogues.[58−60] We therefore also optimized the ground state of complex **Os7** in our DFT calculations in order to determine whether the further inclusion of pyrazine donors into the ligand set would lead to further inverted optoelectronic tuning. Because of problems in converging the ground-state geometry, D_{2d} symmetry was imposed during optimization. The calculated molecular orbital energies confirm the prediction of further stabilization in the energy of the LUMO (−3.30 eV) by 0.15 eV relative to that of **Os6**. However, a more significant stabilization by 0.26 eV of the HOMO is observed (−6.68 eV), leading to enlargement of the HOMO−LUMO gap of **Os7** by 0.12 eV compared to that of **Os6**. On the basis of the trends and correlations of calculated data and their agreement with the experimental electrochemical and spectroscopic data for these complexes, one could confidently predict that the UV−visible absorption and emission profiles of **Os7** would indeed appear further *blue*-shifted compared to those of **Os6**.

The data presented here, complemented with those previously reported for related bidentate systems, show that while the incorporation of pyrazine donors does indeed lead to stabilization of the ligand-based LUMO and a resultant red shift in the optical absorption and emission bands, this is accompanied by stabilization of the HOMO. Increasing the electron-withdrawing character of the ligands may continue to result in red-shifted spectral features until a tipping point is reached, whereby further stabilization of the HOMO exceeds that of the LUMO and is manifested by an inversion in the photophysical tuning behavior. Through sequential modification of the ligand architecture whereby the π-acceptor character is progressively tuned through variation of the number and positions of the pyridine and pyrazine rings, rather than the wholesale replacement of oligopyridyl with oligopyrazinyl-based ligands, we are able to capture this tipping point and the associated inversion in the photophysical properties.

■ CONCLUSIONS

A series of new phosphorescent osmium(II) complexes have been reported that display emission from the red to NIR with the emission intensity sensitive to the presence of oxygen. In pushing the absorption and emission maxima toward the biologically transparent window, the complexes are attractive potential candidate prototypes for the further development of targeted dual-mode theranostic agents for confocal imaging microscopy and photodynamic therapy applications. We will be pursuing this work shortly and will report the results in due course.

Importantly, this systematic survey of the photophysical properties across the series of osmium(II) complexes also reveals an initially unexpected and counterintuitive inversion of spectroscopic tuning with increasing ligand π-acceptor character. While the LUMOs in these complexes are progressively stabilized by this approach, stabilization in the energy of the HOMO is also observed, which reaches a tipping point whereupon stabilization of the latter outcompetes that of the former, leading to an inversion and *blue shifting* in the tuning of the optical absorption and emission properties. This work therefore provides important results with regard to the limitations of photophysical tuning in complexes in which a relatively austere and minimalist electron-withdrawing ligand architecture is incorporated.

■ EXPERIMENTAL SECTION

Os1[36] and benzyl azide[61] were prepared as previously described. ***Caution!*** *Care should be taken in the preparation of triazole-containing compounds utilizing organic azide starting materials because these precursors are potentially explosive.* Minimal C-to-N atom ratios of 2.5:1 to 3:1 are recommended to mitigate this risk if the organic azide is to be isolated prior to use rather than prepared and used in situ. All reagents were purchased from Alfa Aesar, Acros Organics, Sigma-Aldrich, and Fluorochem and used as received. All synthetic manipulations were carried out under an atmosphere of dry N_2 employing standard Schlenk line techniques. Deaeration of solvents (Fisher Scientific) was performed through vigorous bubbling with N_2 for a period of at least 15 min. Dry tetrahydrofuran (THF) was obtained by distillation over CaH_2 and stored under an atmosphere of N_2. Dry *N*,*N*-dimethylformamide (DMF) was purchased from Acros and stored under an atmosphere of dry N_2. NMR spectra were recorded on a Bruker Ascend 400 MHz spectrometer, with all chemical shifts reported in ppm, calibrated relative to the residual solvent signal ($CHCl_3$, ^{1}H δ 7.26, ^{13}C δ 77.16; MeCN, ^{1}H δ 1.94, ^{13}C δ 1.32, 118.26; acetone, ^{1}H δ 2.17, ^{13}C δ 29.84, 206.26). High-resolution mass spectrometry (HRMS) was performed on an Agilent 6210 time-of-flight instrument with a dual electrospray ionization source. Cyclic voltammograms were measured using a PalmSens EmStat3 potentiostat with PSTrace electrochemical software (version 4.8). Analyte solutions (typical concentration 1.5 mmol dm^{-3}) were prepared using N_2-saturated dry MeCN, freshly distilled from CaH_2. All measurements were conducted at RT under a stream of dry N_2 at potential scan rates ranging from 50 to 500 mV s^{-1}. NBu_4PF_6 was used as the supporting electrolyte, being recrystallized from EtOH and oven-dried prior to use, with a typical solution concentration of 0.2 mol dm^{-3}. The working electrode was glassy carbon, with platinum wire utilized as the counter electrode. The reference electrode was Ag/AgCl, being chemically isolated from the analyte solution by an electrolyte-containing bridge tube tipped with a porous frit. Ferrocene was employed as an internal reference, with all potentials quoted relative to the Fc^+/Fc couple. UV−visible electronic absorption spectra were recorded on an Agilent Cary-60 spectrophotometer, utilizing quartz cuvettes of 1 cm path length. Emission spectra were recorded on a Fluoromax-4 spectrophotometer utilizing quartz cuvettes of 1 cm path length and corrected for both the detector response and solvent Raman signals. "Degassed" solutions were prepared via three repeat "freeze−pump−thaw" cycles. Quantum yields (Φ_{em}) are quoted relative to $[Ru(bpy)_3][PF_6]_2$ in aerated MeCN, with all complexes being excited at a single wavelength with common optical density. Quantum yields are thus determined from the ratio of the integrated area under the peaks. Because emission bands for the osmium complexes tail into the NIR region, outside the effective range of the spectrophotometer, an experimental uncertainty of ±20% is assumed. Luminescence lifetimes were measured with an Edinburgh Instruments Mini-τ, equipped with a picosecond diode laser (404 nm, 56 ps) excitation source.

Synthesis of 2,6-Bis(ethynyltrimethylsilyl)pyrazine (2). 2,6-Dibromopyrazine (1.50 g, 6.30 mmol), $Pd(PPh_3)_2Cl_2$ (233 mg, 0.33 mmol, 5 mol %), and CuI (127 mg, 0.66 mmol, 10 mol %) were added to a deaearated mixture of dry THF/Et_3N (1:1, v/v; 50 mL). Ethynyltrimethylsilane (3.6 mL, ρ = 0.709 g mL^{-1}, 25.9 mmol) was added and the reaction solution stirred at 50 °C for 16 h. The reaction solution was cooled to RT and filtered through a short silica pad (2 cm) and the filtrate reduced in volume. Purification was achieved via column chromatography (SiO_2, CH_2Cl_2). Yield: 1.11 g, 65%. ^{1}H NMR ($CDCl_3$, 400 MHz): δ 0.27 (s, 18H), 8.54 (s, 2H). ^{13}C NMR ($CDCl_3$, 101 MHz): δ −0.35, 100.26, 100.45, 139.32, 146.00. HRMS (ESI). Calcd for $C_{14}H_{21}N_2Si_2$ (MH^+): m/z 273.1243. Found: m/z 273.1244.

Synthesis of 2,6-Bis(1-benzyl-1,2,3-triazol-4-yl)pyrazine (3). **2** (1.10 g, 4.03 mmol), $CuSO_4{\cdot}5H_2O$ (0.77 g, 3.07 mmol), sodium ascorbate (1.22, 6.16 mmol), K_2CO_3 (3.56 g, 25.7 mmol), and benzyl azide (1.37 g, 10.3 mmol) were combined in 1:1 (v/v) THF/H_2O (100 mL). *tert*-Butyl alcohol (^{t}BuOH; 20 mL) and pyridine (3.5 mL)

DOI: 10.1021/acs.inorgchem.9b00915
Inorg. Chem. XXXX, XXX, XXX−XXX

were added and the resultant mixture stirred at RT for 16 h. The organic solvents were removed by rotary evaporation to leave an aqueous suspension, to which was added $CHCl_3$ (150 mL), additional H_2O (60 mL), and concentrated aqueous NH_3 (15 mL). The biphasic mixture was stirred rapidly at RT for 1 h. The organic layer was separated, washed successively with dilute aqueous NH_3 (200 mL), saturated brine (200 mL), and H_2O (200 mL), then dried over $MgSO_4$, and evaporated to dryness. Purification was performed via column chromatography (SiO_2, 1% $MeOH/CH_2Cl_2$), affording the title compound as a white solid. Yield: 1.25 g, 79%. ^{1}H NMR ($CDCl_3$, 400 MHz): δ 5.59 (s, 4H), 7.26−7.34 (m, 4H), 7.34−7.43 (m, 6H), 8.05 (s, 2H), 9.30 (s, 2H). ^{13}C NMR ($CDCl_3$, 101 MHz): δ 54.56, 122.97, 128.25, 129.08, 129.36, 134.37, 140.87, 144.91, 146.36. HRMS (ESI). Calcd for $C_{22}H_{19}N_8$ (MH^+): m/z 395.1727. Found: m/z 395.1729. Calcd for $C_{22}H_{18}N_8Na$ (M + Na^+): m/z 417.1547. Found: m/z 417.1547. Anal. Calcd for $C_{22}H_{18}N_8$: C, 66.99; H, 4.60; N, 28.41. Found: C, 66.98; H, 4.42;N, 28.29.

Synthesis of 2-(Tri-*n*-butylstannyl)pyridine (4). The synthesis was carried out following a previously published procedure:[62] To a solution of 2-bromopyridine (3 mL, ρ = 1.657 g mL^{-1}, 31.5 mmol) in dry THF (120 mL) at −78 °C was added, dropwise, ^{n}BuLi (13.3 mL, 2.5 M in hexanes, 33.3 mmol). The mixture was stirred for a further 1 h at −78 °C before the quick addition of tri-*n*-butyltin chloride (8.6 mL, ρ = 1.2 g mL^{-1}, 31.7 mmol). Stirring was maintained at −78 °C for 3 h before the solution was allowed to warm to RT and then quenched through the addition of a saturated aqueous solution of NH_4Cl (30 mL). The reaction mixture was extracted into ethyl acetate (3 × 50 mL) with the combined organic layers, then washed with saturated brine (100 mL) and H_2O (100 mL), and dried over $MgSO_4$. Evaporation of the solvent in vacuo yielded a light-brown oil, which was stored in the refrigerator and used without further purification. Yield: 11.30 g, 97%. Characterization data matched those previously reported.[62] ^{1}H NMR ($CDCl_3$, 400 MHz): δ 0.84−0.90 (m, 9H), 1.08−1.14 (m, 6H), 1.28−1.37 (m, 6H), 1.50−1.59 (m, 6H), 7.10 (ddd, J = 1.3, 4.9, and 7.7 Hz, 1H), 7.39 (dt, J = 1.2 and 7.4 Hz, 1H), 7.48 (td, J = 1.7 and 7.5 Hz, 1H), 8.73 (d, J = 4.8 Hz, 1H).

Synthesis of 6-Bromo-2,2′-bipyridine (5). 2,6-Dibromopyridine (5.69 g, 24.0 mmol), **4** (8.00 g, 21.7 mmol), and $Pd(PPh_3)_4$ (1.50 g, 1.30 mmol, 6 mol %) were combined in thoroughly deaerated toluene (30 mL) and heated to reflux for 12 h. After cooling to RT, the solvent was removed by rotary evaporation and the resulting residue redissolved in CH_2Cl_2 (30 mL). Extraction of the organic phase with 3 × 50 mL portions of 6 M aqueous HCl provided an aqueous solution that was subsequently neutralized with 10% aqueous NH_3 solution. The aqueous phase was then extracted with CH_2Cl_2 (3 × 30 mL), with the combined organic layers being washed with H_2O (100 mL), dried over $MgSO_4$, and evaporated to dryness. Purification was achieved via column chromatography (SiO_2, gradient elution, 0.5% $MeOH/CH_2Cl_2$ to 1% $MeOH/CH_2Cl_2$), affording the product as a white solid. Yield: 1.38 g, 27%. ^{1}H NMR ($CDCl_3$, 400 MHz): δ 7.30−7.35 (m, 1H), 7.49 (d, J = 7.8 Hz, 1H), 7.66 (t, J = 8.00 Hz, 1H), 7.82 (td, J = 1.6 and 7.9 Hz, 1H), 8.35−8.43 (m, 2H), 8.66 (d, J = 4.5 Hz, 1H). ^{13}C NMR ($CDCl_3$, 101 MHz): δ 119.86, 121.64, 124.41, 128.13, 137.17, 139.37, 141.74, 149.37, 154.64, 157.50. HRMS (ESI). Calcd for $C_{10}H_8N_2Br$ (MH^+): m/z 234.9865. Found: m/z 234.9867.

Synthesis of 6-(Ethynyltrimethylsilyl)-2,2′-bipyridine (6). **5** (1.22 g, 5.19 mmol), $Pd(PPh_3)_2Cl_2$ (182 mg, 0.26 mmol, 5 mol %), and CuI (99 mg, 0.52 mmol, 10 mol %) were added to a deaerated 1:1 (v/v) mixture of dry THF/Et_3N (60 mL). Ethynyltrimethylsilane (1.8 mL, ρ = 0.709 g mL^{-1}, 13.0 mmol) was added and the reaction solution then heated to 60 °C for 16 h. The reaction mixture was allowed to cool to RT and passed through a short (2 cm) silica pad and the filtrate evaporated. The residue was purified via column chromatography (SiO_2, 1% $MeOH/CH_2Cl_2$), affording the title compound. Yield: 1.09 g, 83%. ^{1}H NMR ($CDCl_3$, 400 MHz): δ 0.29 (s, 9H), 7.27−7.34 (m, 1H), 7.48 (d, J = 7.6 Hz, 1H), 7.73−7.83 (m, 2H), 8.35 (d, J = 8.0 Hz, 1H), 8.47 (d, J = 8.0 Hz, 1H), 8.65 (d, J = 4.4 Hz, 1H). ^{13}C NMR ($CDCl_3$, 101 MHz): δ −0.08, 94.61, 104.12, 120.67, 121.74, 124.10, 127.68, 137.01, 137.08, 142.58, 149.18, 155.54, 156.58. HRMS (ESI). Calcd for $C_{15}H_{17}N_2Si$ (MH^+): m/z 253.1161. Found: m/z 253.1156.

Synthesis of 6-(1-Benzyl-1,2,3-triazol-4-yl)-2,2′-bipyridine (7). **6** (1.10 g, 4.36 mmol), benzyl azide (0.57 g, 4.29 mmol), K_2CO_3 (1.19 g, 8.62 mmol), $CuSO_4{\cdot}5H_2O$ (0.42 g, 1.69 mmol), and sodium ascorbate (0.68 g, 3.43 mmol) were added to 1:1 (v/v) THF/H_2O (100 mL). ^{t}BuOH (20 mL) and pyridine (3.5 mL) were added, and the reaction mixture was then stirred for 16 h at RT. The organic solvents were removed by rotary evaporation to afford an aqueous suspension, to which was added $CHCl_3$ (100 mL), additional H_2O (50 mL), and concentrated aqueous NH_3 (15 mL). The biphasic mixture was stirred rapidly at RT for 40 min and the organic layer then separated. The organic phase was washed successively with dilute aqueous NH_3 (200 mL) and brine (200 mL), followed by H_2O (200 mL), and then dried over $MgSO_4$. Purification was carried out via column chromatography (Al_2O_3, gradient elution, CH_2Cl_2 to 2% $MeOH/CH_2Cl_2$), giving the product as a white solid. Yield: 0.59 g, 44%. ^{1}H NMR ($CDCl_3$, 400 MHz): δ 5.62 (s, 2H), 7.27−7.43 (m, 6H), 7.79 (td, J = 1.2 and 7.8 Hz, 1H), 7.90 (t, J = 7.9 Hz, 1H), 8.17 (s, 1H), 8.20 (dd, J = 0.8 and 7.9 Hz, 1H), 8.32 (dd, J = 0.8 and 7.7 Hz, 1H), 8.40 (d, J = 7.9 Hz, 1H), 8.67 (d, J = 4.3 Hz, 1H). ^{13}C NMR ($CDCl_3$, 101 MHz): 54.49, 120.29, 120.32, 121.19, 122.19, 123.90, 128.23, 128.94, 129.31, 134.74, 136.90, 137.96, 149.23, 149.33, 149.76, 155.82, 156.07. HRMS (ESI). Calcd for $C_{19}H_{16}N_5$ (MH^+): m/z 314.1400. Found: m/z 314.1402. Calcd for $C_{19}H_{15}N_5Na$ (M + Na^+): m/z 336.1220. Found: m/z 336.1220. Anal. Calcd for $C_{19}H_{15}N_5$: C, 72.83; H, 4.83; N, 22.35. Found: C, 72.94; H, 4.86; N, 22.43.

Synthesis of 2-Bromo-6-(pyridin-2-yl)pyrazine (8). 2,6-Dibromopyrazine (3.55 g, 14.9 mmol), 2-(tributylstannyl)pyridine (5.51 g, 14.9 mmol), and $Pd(PPh_3)_4$ (1.07 g, 0.926 mmol, 6 mol %) were added to deaerated toluene (100 mL) and heated at 110 °C for 21 h. The dark-red-brown mixture was cooled to RT and the solvent removed under reduced pressure. The resulting oily residue was redissolved in CH_2Cl_2 (100 mL) and extracted with 2 × 100 mL portions of aqueous 6 M HCl. The combined aqueous layers were then neutralized with a 30% aqueous NH_3 solution, resulting in the formation of a light-brown precipitate. The aqueous suspension was extracted with 2 × 100 mL portions of CH_2Cl_2, with the combined organic phases then being dried over $MgSO_4$ and the solvent removed. Purification was achieved via column chromatography (SiO_2, gradient elution 0.5% $MeOH/CH_2Cl_2$ to 0.75% $MeOH/CH_2Cl_2$), with the product eluting immediately before a yellow band. The title compound was obtained as a white solid. Yield: 1.50 g, 43%. ^{1}H NMR ($CDCl_3$, 400 MHz): δ 7.38 (ddd, J = 1.2, 4.7, and 7.5 Hz, 1H), 7.85 (td, J = 1.8 and 7.7 Hz, 1H), 8.36 (d, J = 8.0 Hz, 1H), 8.68−8.72 (m, 2H), 9.56 (s, 1H). ^{13}C NMR ($CDCl_3$, 101 MHz): δ 122.08, 125.09, 137.32, 140.08, 141.03, 147.03, 149.72, 151.90, 152.87. HRMS (ESI). Calcd for $C_9H_7N_3Br$ (MH^+): m/z 235.9818. Found: m/z 235.9823.

2-(Ethynyltrimethylsilyl)-6-(pyridin-2-yl)pyrazine (9). **8** (1.36 g, 5.76 mmol), $Pd(PPh_3)_2Cl_2$ (215 mg, 0.307 mmol, 5 mol %), and CuI (102 mg, 0.536 mmol, 9 mol %) were added to deaerated 1:1 (v/v) dry THF/Et_3N (80 mL). Ethynyltrimethylsilane (1.6 mL, ρ = 0.709 g mL^{-1}, 11.5 mmol) was added and the reaction mixture then stirred at 60 °C for 16 h. The resultant dark-brown solution was filtered through a short silica pad and the filtrate evaporated to dryness. Purification was carried out via column chromatography (SiO_2, 1% $MeOH/CH_2Cl_2$), affording the product as a pale-yellow oil. Yield: 1.14 g, 78%. ^{1}H NMR ($CDCl_3$, 400 MHz): δ 0.31 (s, 9H), 7.37 (ddd, J = 0.8, 4.8, and 7.5 Hz, 1H), 7.84 (td, J = 1.7 and 7.7 Hz, 1H), 8.42 (d, J = 7.9 Hz, 1H), 8.68−8.73 (m, 2H), 9.53 (s, 1H). ^{13}C NMR ($CDCl_3$, 101 MHz): δ −0.21, 99.50, 101.14, 122.05, 124.81, 137.20, 138.51, 141.71, 147.54, 149.56, 150.64, 153.72. HRMS (ESI). Calcd for $C_{14}H_{16}N_3Si$ (MH^+): m/z 254.1108. Found: m/z 254.1117.

2-(1-Benzyl-1,2,3-triazol-4-yl)-6-(pyridin-2-yl)pyrazine (10). **9** (1.14 g, 4.50 mmol) and benzyl azide (610 mg, 4.58 mmol) were added to 1:1 (v/v) THF/H_2O (120 mL). ^{t}BuOH (20 mL) was added, followed by K_2CO_3 (1.08 g, 7.82 mmol), $CuSO_4{\cdot}5H_2O$ (463 mg, 1.85 mmol), sodium ascorbate (768 mg, 3.87 mmol), and

DOI: 10.1021/acs.inorgchem.9b00915
Inorg. Chem. XXXX, XXX, XXX−XXX

pyridine (3.5 mL). The reaction mixture was stirred rapidly at RT for 27 h, and the organic solvents were then removed via rotary evaporation. To the resulting aqueous suspension was then added $CHCl_3$ (150 mL), additional H_2O (50 mL), and concentrated aqueous NH_3 (12 mL). The biphasic mixture was stirred rapidly at RT for 1 h and the organic layer separated. The aqueous phase was extracted with further 2 × 50 mL portions of $CHCl_3$, with the combined organic layers then being washed successively with dilute aqueous NH_3 (2 × 100 mL), brine (1 × 100 mL), and H_2O (100 mL). The organic phase was dried over $MgSO_4$ and the solvent removed to leave a light-brown solid, which was purified by column chromatography (SiO_2, gradient elution 1% $MeOH/CH_2Cl_2$ to 2.5% $MeOH/CH_2Cl_2$), affording the product as an off-white solid after thorough drying in vacuo. Yield: 1.09 g, 77%. ^{1}H NMR ($CDCl_3$, 400 MHz): δ 5.64 (s, 2H), 7.33−7.45 (m, 6H), 7.82 (td, J = 1.7 and 7.7 Hz, 1H), 8.18 (s, 1H), 8.35 (d, J = 7.9 Hz, 1H), 8.71 (d, J = 4.6 Hz, 1H), 9.43 (s, 1H), 9.54 (s, 1H). ^{13}C NMR ($CDCl_3$, 101 MHz): δ 54.46, 121.43, 123.02, 124.49, 128.15, 128.96, 129.25, 134.34, 136.96, 141.44, 141.89, 144.43, 146.56, 149.48, 149.96, 153.97. HRMS (ESI). Calcd for $C_{18}H_{15}N_6$ (MH^+): m/z 315.1353. Found: m/z 315.1381. Calcd for $C_{18}H_{14}N_6Na$ (M + Na^+): m/z 337.1172. Found: m/z 337.1174.

Synthesis of 2-Pyrazinyl *N*-Methyliminodiacetic Acid Boronate (11). Following the procedure previously reported by Burke and co-workers,[50] 2-iodopyrazine (2.0 mL, ρ = 2.086 g mL^{-1}, 20.2 mmol) and triisopropyl borate (4.7 mL, ρ = 0.815 g mL^{-1}, 20.3 mmol) were added to dry THF (70 mL) and cooled to −78 °C. ^{n}BuLi (8.1 mL, 2.5 M in hexanes, 20.2 mmol) was added dropwise and the solution stirred for 1 h at −78 °C and then allowed to warm to RT with further stirring for 3 h. Separately, a three-necked flask equipped with a dropping funnel, a thermometer, and a distillation apparatus was charged, under N_2, with a previously prepared solution of *N*-methyliminodiacetic acid (5.35 g, 36.3 mmol) in dimethyl sulfoxide (DMSO; 30 mL), which was subsequently heated to 120 °C. The boronate solution was then transferred via cannula to the dropping funnel and added to the hot reaction mixture slowly, dropwise, at such a rate so as to maintain the internal temperature between 110 and 120 °C. THF was rapidly distilled during the course of the addition, after which the DMSO solvent was also removed by distillation under reduced pressure at 50 °C. The resulting brown residue was dried under high vacuum overnight at 50 °C. Purification was carried out by column chromatography (SiO_2, gradient elution, 5% $MeCN/Et_2O$ to MeCN), affording the product as a light-brown crystalline solid, which was stored in the refrigerator. Yield: 2.50 g, 53%. Characterization data matched those previously reported.[50] ^{1}H NMR (MeCN-d_3, 400 MHz): δ 2.61 (s, 3H), 4.00 (d, J = 16.6 Hz, 2H), 4.18 (d, J = 16.9 Hz, 2H), 8.53 (d, J = 2.6 Hz, 1H), 8.68 (dd, J = 1.6 and 2.6 Hz, 1H), 8.77 (d, J = 1.6 Hz, 1H).

Synthesis of 2-Bromo-6-(1-benzyl-1,2,3-triazol-4-yl)-pyridine (13). 2,6-Dibromopyridine (5.00 g, 21.1 mmol), $Pd(PPh_3)_2Cl_2$ (730 mg, 1.04 mmol, 5 mol %), and CuI (403 mg, 2.11 mmol, 10 mol %) were added to a deaerated 7:1 (v/v) mixture of dry THF/Et_3N (80 mL). Ethynyltrimethylsilane (2.65 mL, ρ = 0.709 g mL^{-1}, 19.1 mmol) was added and the reaction solution stirred at 40 °C for 6 h. The dark-brown solution was cooled to RT and passed through a short (2 cm) silica plug and the filtrate evaporated to dryness. Column chromatography (SiO_2, 3:7 CH_2Cl_2/hexane) afforded a white solid (1.95 g), which was found by ^{1}H NMR ($CDCl_3$) analysis to contain a mixture of the desired 2-bromo-6-(ethynyltrimethylsilyl)pyridine (**12**) and a small quantity of unreacted 2,6-dibromopyridine, which was used in the subsequent step without further purification, as has been previously reported.[63] **12** (1.27 g, mixture as detailed above), benzyl azide (0.69 g, 5.18 mmol), and K_2CO_3 (1.55 g, 11.2 mmol) were added to 1:1 (v/v) THF/H_2O (120 mL). ^{t}BuOH (20 mL) was added, followed by $CuSO_4{\cdot}5H_2O$ (0.65 g, 2.60 mmol), sodium ascorbate (1.00 g, 5.04 mmol), and pyridine (3 mL). The reaction mixture was stirred at RT for 23 h, after which the organic solvents were removed by rotary evaporation. To the resulting aqueous suspension was then added $CHCl_3$ (150 mL), additional H_2O (50 mL), and concentrated aqueous NH_3 (12 mL). The biphasic mixture was stirred rapidly for 1 h at RT. The organic layer was removed and the aqueous phase extracted with a 50 mL portion of $CHCl_3$. The combined organic layers were washed with dilute aqueous NH_3 (100 mL), followed by brine (100 mL), dried over $MgSO_4$, and then evaporated to dryness. The crude solids were purified by column chromatography (SiO_2, 1% $MeOH/CH_2Cl_2$) to give the title compound as a white powder. Yield: 0.73 g, 46%. ^{1}H NMR ($CDCl_3$, 400 MHz): δ 5.56 (s, 2H), 7.28−7.35 (m, 2H), 7.35−7.42 (m, 4H), 7.60 (t, J = 7.7 Hz, 1H), 8.08 (s, 1H), 8.12 (dd, J = 0.6 and 7.7 Hz, 1H). ^{13}C NMR ($CDCl_3$, 101 MHz): δ 54.57, 118.94, 122.79, 127.09, 128.40, 129.07, 129.34, 134.32, 139.30, 141.75, 147.55, 151.44. HRMS (ESI). Calcd for $C_{14}H_{12}N_4Br$ (MH^+): m/z 315.0240. Found: m/z 315.0233. Calcd for $C_{14}H_{11}N_4BrNa$ (M + Na^+): m/z 337.0059. Found: m/z 337.0053.

Synthesis of 2-Pyrazinyl-6-(1-benzyl-1,2,3-triazol-4-yl)-pyridine (14). Anhydrous $Cu(OAc)_2$ (146 mg, 0.80 mmol), tribasic K_3PO_4 (780 mg, 3.68 mmol), and 10 4 Å molecular sieves were added to thoroughly deaerated dry DMF (20 mL). Diethanolamine (160 μL, ρ = 1.097 g mL^{-1}, 1.67 mmol) was added and the mixture heated to 85 °C for 15 min. The resulting deep-blue mixture was then transferred via cannula to a reaction flask containing **13** (435 mg, 1.38 mmol), **11** (575 mg, 2.44 mmol), tribasic K_3PO_4 (790 mg, 3.72 mmol), anhydrous KOAc (146 mg, 1.49 mmol), Pd XPhos G1 (77 mg, 0.10 mmol), and 10 4 Å molecular sieves. The reaction mixture was heated to 100 °C for 20 h, cooled to RT, and then diluted through the addition of $CHCl_3$ (100 mL) and H_2O (150 mL). The organic layer was separated and the aqueous phase extracted with a further 100 mL portion of $CHCl_3$. The combined organic layers were then washed with H_2O (2 × 200 mL), dilute aqueous NH_3 (2 × 100 mL), followed by brine (100 mL), dried over $MgSO_4$, and then evaporated to dryness. Purification was carried out by column chromatography (Al_2O_3, gradient elution, 0.1% $MeOH/CH_2Cl_2$ to 0.2% $MeOH/CH_2Cl_2$), giving the product as a white solid. Yield: 194 mg, 45%. ^{1}H NMR ($CDCl_3$, 400 MHz): δ 5.62 (s, 2H), 7.32−7.44 (m, 5H), 7.91 (t, J = 7.9 Hz, 1H), 8.16 (s, 1H), 8.24 (dd, J = 0.8 and 8.0 Hz, 1H), 8.26 (dd, J = 0.8 and 8.0 Hz, 1H), 8.57 (d, J = 2.5 Hz, 1H), 8.58−8.60 (m, 1H), 9.62 (d, J = 1.3 Hz, 1H). ^{13}C NMR ($CDCl_3$, 101 MHz): δ 54.53, 120.55, 120.90, 122.35, 128.29, 129.01, 129.34, 134.57, 138.13, 143.42, 143.70, 144.58, 148.81, 150.08, 150.99, 153.82. HRMS (ESI). Calcd for $C_{18}H_{15}N_6$ (MH^+): m/z 315.1353. Found: m/z 315.1350. Calcd for $C_{18}H_{14}N_6Na$ (M + Na^+): m/z 337.1172. Found: m/z 337.1164. Anal. Calcd for $C_{18}H_{14}N_6$: C, 68.78; H, 4.49; N, 26.73. Found: C, 68.89; H, 4.57; N, 26.61.

2-Bromo-6-(1-benzyl-1,2,3-triazol-4-yl)pyrazine (16). 2,6-Dibromopyrazine (7.00 g, 29.4 mmol), $Pd(PPh_3)_2Cl_2$ (0.94 g, 1.34 mmol, 4.5 mol %), and CuI (0.51 g, 2.68 mmol, 9.1 mol %) were added to a mixture of dry THF (75 mL) and Et_3N (15 mL). Ethynyltrimethylsilane (4.1 mL, ρ = 0.709 g mL^{-1}, 29.6 mmol) was added and the reaction solution heated to 30 °C for 6 h. The dark-red-brown solution was cooled to RT and filtered through a short silica pad. The filtrate was evaporated to dryness and the resultant residue subjected to column chromatography (SiO_2, 7:3 hexane/CH_2Cl_2), affording an orange oil. ^{1}H NMR analysis revealed the product to be comprised of a mixture of 2,6-dibromopyrazine, **2**, and 2-bromo-6-(ethynyltrimethylsilyl)pyrazine (**15**) in a 0.5:0.5:1 respective molar ratio. This mixture was used in the following step without further purification. Yield (based on **15**): 2.90 g, 39%. Relevant ^{1}H NMR ($CDCl_3$, 400 MHz) analysis for **15**: δ 0.28 (s, 9H), 8.58 (s, 1H), 8.59 (s, 1H).

The above mixture of substituted pyrazines (5.50 g, calcd to contain 2.75 g, 10.8 mmol, of **15**) was combined with excess benzyl azide (3.31 g, 24.9 mmol), $CuSO_4{\cdot}5H_2O$ (2.75 g, 11.0 mmol), sodium ascorbate (4.12 g, 20.7 mmol), and K_2CO_3 (5.00 g, 36.23 mmol) in a 1:1 (v/v) solution of THF/H_2O (300 mL). ^{t}BuOH (30 mL) was added, followed by pyridine (6 mL), and the resultant suspension stirred rapidly at RT for 18 h. The organic solvent was removed by rotary evaporation to give an aqueous suspension, to which was added $CHCl_3$ (200 mL), concentrated aqueous NH_3 (20 mL), and additional H_2O (50 mL). The biphasic mixture was stirred rapidly at RT for 1 h and the organic layer then removed. The aqueous phase

DOI: 10.1021/acs.inorgchem.9b00915
Inorg. Chem. XXXX, XXX, XXX−XXX

was extracted with a further 100 mL portion of $CHCl_3$, and the combined organic layers were then washed successively with dilute aqueous NH_3 (10%; 2 × 100 mL) and brine (1 × 100 mL). The organic phase was dried over $MgSO_4$ and the solvent removed to leave an oily residue, which was purified by column chromatography (SiO_2, 1.5% MeOH/CH_2Cl_2), yielding the title compound as a white solid. Yield: 2.39 g, 70%. ^{1}H NMR ($CDCl_3$, 400 MHz): δ 5.59 (s, 2H), 7.29−7.35 (m, 2H), 7.36−7.43 (m, 3H), 8.10 (s, 1H), 8.57 (s, 1H), 9.33 (s, 1H). ^{13}C NMR ($CDCl_3$, 101 MHz): δ 54.66, 123.71, 128.40, 129.20, 129.40, 134.02, 139.75, 140.17, 145.12, 145.98, 146.41. HRMS (ESI). Calcd for $C_{13}H_{11}N_5Br$ (MH^+): m/z 316.0192. Found: m/z 316.0190. Calcd for $C_{13}H_{10}N_5BrNa$ (M + Na^+): m/z 338.0012. Found: m/z 338.0011. Calcd for $C_{26}H_{20}N_{10}Br_2Na$ (2M + Na^+): m/z 653.0132. Found: m/z 653.0087.

Synthesis of 6-(1-Benzyl-1,2,3-triazol-4-yl)-2,2′-bipyrazine (17). Anhydrous $Cu(OAc)_2$ (200 mg, 1.10 mmol) and tribasic K_3PO_4 (970 mg, 4.57 mmol) were added to dry, thoroughly deaerated DMF (20 mL) along with 10 4 Å molecular sieves. Diethanolamine (210 μL, ρ = 1.097 g mL^{-1}, 2.19 mmol) was added and the solution heated to 85 °C with stirring for 10 min. The resulting bright-blue solution was then transferred via cannula to a reaction vessel containing **16** (608 mg, 1.92 mmol), **11** (661 mg, 2.81 mmol), tribasic K_3PO_4 (800 mg, 3.77 mmol), anhydrous KOAc (184 mg, 1.87 mmol), Pd XPhos G1 (97 mg, 0.13 mmol), and 10 4 Å molecular sieves. The reaction mixture was heated to 100 °C for 22 h, cooled to RT, and then diluted through the addition of $CHCl_3$ (100 mL) and H_2O (150 mL). The organic layer was removed and the aqueous phase extracted with a further portion (100 mL) of $CHCl_3$. The combined organic layers were washed successively with H_2O (200 mL), dilute aqueous NH_3 (2 × 100 mL), followed by brine (100 mL), dried over $MgSO_4$ and the solvent was removed in vacuo. The residue was purified by column chromatography (Al_2O_3, 0.1% MeOH/CH_2Cl_2), giving an off-white powder. The solids were redissolved in CH_2Cl_2 (15 mL) and slowly triturated with excess hexanes to afford the pure title compound as a white solid. Yield: 128 mg, 21%. ^{1}H NMR (acetone-d_6, 400 MHz): δ 5.79 (s, 2H), 7.33−7.45 (m, 3H), 7.45−7.50 (m, 2H), 8.72−8.75 (m, 2H), 8.91 (s, 1H), 9.37 (s, 1H), 9.44 (s, 1H), 9.62 (d, J = 0.9 Hz, 1H). ^{13}C NMR (acetone-d_6, 101 MHz): δ 54.71, 125.36, 129.09, 129.37, 129.88, 136.82, 142.27, 142.65, 144.20, 145.03, 146.11, 146.59, 146.71, 149.28, 149.99. HRMS (ESI). Calcd for $C_{17}H_{14}N_7$ (MH^+): m/z 316.1305. Found: m/z 316.1296. Calcd for $C_{17}H_{13}N_7Na$ (M + Na^+): m/z 338.1125. Found: m/z 338.1116. Anal. Calcd for $C_{17}H_{13}N_7$: C, 64.75; H, 4.16; N, 31.09. Found: C, 64.81; H, 3.96; N, 31.03.

Synthesis of 2,2′:6′,2″-Terpyrazine (18). 2,6-Dibromopyrazine (325 mg, 1.36 mmol), **11** (1.11 g, 4.72 mmol), tribasic K_3PO_4 (2.14 g, 10.1 mmol), Pd XPhos G1 (80 mg, 0.11 mmol), anhydrous $Cu(OAc)_2$ (274 mg, 1.51 mmol), diethanolamine (0.3 mL, ρ = 1.097 g mL^{-1}, 3.13 mmol), and 20 4 Å molecular sieves were added to an oven-dried flask. Dry, deaerated DMF (15 mL) was added and the mixture heated to 100 °C for 17 h. After cooling to RT, the mixture was diluted through the addition of $CHCl_3$ (70 mL) and H_2O (100 mL). The organic phase was removed and the aqueous layer extracted with a further 50 mL portion of $CHCl_3$. The combined organic layers were subsequently washed with dilute aqueous NH_3 (100 mL), followed by brine (2 × 200 mL), and dried over $MgSO_4$. The solvent was removed under reduced pressure, and the remaining brown solids were dried thoroughly under high vacuum. The crude solids were then suspended in stirring MeOH (30 mL), collected by filtration, and washed with hexane to give the pure title compound as beige solids. Yield: 89 mg, 28%. NMR characterization was found to be in agreement with that reported in the literature.[38] ^{1}H NMR ($CDCl_3$, 400 MHz): δ 8.71 (s, 4H), 9.68 (s, 2H), 9.75 (s, 2H). HRMS (ESI). Calcd for $C_{12}H_9N_6$ (MH^+): m/z 237.0888. Found: m/z 237.0887.

Synthesis of Os2. [$(NH_4)_2OsCl_6$] (150 mg, 0.34 mmol) and **3** (282 mg, 0.72 mmol) were combined in ethylene glycol (25 mL) and heated to reflux for 16 h. The reaction mixture was cooled to RT and treated with an aqueous solution (25 mL) of NH_4PF_6 (165 mg, 1.01 mmol). The resulting dark-colored precipitate was collected by filtration, washed with H_2O, followed by Et_2O, and dried in vacuo. The solids were recrystallized from CH_2Cl_2/hexanes, giving the title complex as a dark-brown powder. Yield: 347 mg, 80%. ^{1}H NMR (MeCN-d_3, 400 MHz): δ 5.37 (s, 8H), 7.15 (d, J = 7.3 Hz, 8H), 7.28−7.41 (m, 12H), 8.66 (s, 4H), 9.28 (s, 4H). ^{13}C NMR (MeCN-d_3, 101 MHz): δ 56.73, 127.70, 129.42, 130.10, 130.18, 133.84, 140.57, 145.78, 149.48. HRMS (ESI). Calcd for $[C_{44}H_{36}N_{16}Os]^{2+}$ (M^{2+}): m/z 490.1456. Found: m/z 490.1457. Anal. Calcd for $C_{44}H_{36}N_{16}P_2F_{12}Os$: C, 41.64; H, 2.86; N, 17.66. Found: C, 41.77; H, 2.67; N, 17.76.

Synthesis of Os3. [$(NH_4)_2OsCl_6$] (150 mg, 0.34 mmol) and **7** (225 mg, 0.72 mmol) were combined in ethylene glycol (25 mL) and heated to reflux for 16 h. The reaction mixture was cooled to RT and treated with an aqueous solution (25 mL) of NH_4PF_6 (275 mg, 1.69 mmol). The resulting dark-green precipitate was collected by filtration, washed with H_2O, and dried in vacuo. The solids were purified by column chromatography (Al_2O_3, 4:1 CH_2Cl_2/MeCN), followed by recrystallization from MeCN/Et_2O, giving the desired complex as a dark-green powder. Yield: 100 mg, 27%. ^{1}H NMR (MeCN-d_3, 400 MHz): δ 5.33 (s, 4H), 7.06−7.13 (m, 6H), 7.23 (d, J = 5.5 Hz, 2H), 7.26−7.38 (m, 6 H), 7.76 (td, J = 1.5 and 7.8 Hz, 2H), 7.87 (t, J = 8.0 Hz, 2H), 8.34 (d, J = 8.0 Hz, 2H), 8.39 (d, J = 8.0 Hz, 2H), 8.55 (s, 2H), 8.56 (d, J = 8.0 Hz, 2H). ^{13}C NMR (MeCN-d_3, 101 MHz): δ 56.44, 121.44, 121.73, 125.40, 127.20, 128.51, 129.21, 130.00, 130.02, 134.15, 136.94, 138.53, 150.99, 151.97, 153.30, 156.92, 161.11. HRMS (ESI). Calcd for $[C_{38}H_{30}N_{10}Os]^{2+}$ (M^{2+}): m/z 409.1129. Found: m/z 409.1148. Anal. Calcd for $C_{38}H_{30}N_{10}P_2F_{12}Os$: C, 41.23; H, 2.73; N, 12.65. Found: C, 41.20; H, 2.69; N, 12.57.

Synthesis of Os4. [$(NH_4)_2OsCl_6$] (153 mg, 0.35 mmol) and **10** (236 mg, 0.75 mmol) were combined in ethylene glycol (20 mL) and heated to reflux for 17 h. The reaction mixture was cooled to RT and treated with an aqueous solution (10 mL) of NH_4PF_6 (337 mg, 2.06 mmol). The resulting dark-green precipitate was collected by filtration, washed with H_2O, followed by Et_2O, and dried in vacuo. The solids were purified by column chromatography [SiO_2, 1:1:10 (v/v/v) H_2O/saturated aqueous KNO_3/MeCN], which after subsequent counterion metathesis gave the title complex as a dark-green powder. Yield: 172 mg, 45%. ^{1}H NMR (MeCN-d_3, 400 MHz): δ 5.35 (s, 4H), 7.08−7.21 (m, 6H), 7.23−7.40 (m, 8H), 7.86 (t, J = 7.6 Hz, 2H), 8.57 (d, J = 7.9 Hz, 2H), 8.66 (s, 2H), 9.38 (s, 2H), 9.64 (s, 2H). ^{13}C NMR (MeCN-d_3, 101 MHz): δ 56.68, 125.86, 127.65, 128.75, 129.39, 130.02, 130.09, 133.80, 139.64, 141.94, 142.62, 144.63, 149.05, 150.41, 154.40, 158.59. HRMS (ESI). Calcd for $[C_{36}H_{28}N_{12}Os]^{2+}$ (M^{2+}): m/z 410.1082. Found: m/z 410.1090. Anal. Calcd for $C_{36}H_{28}N_{12}OsP_2F_{12}$: C, 38.99; H, 2.55; N, 15.16. Found: C, 38.88; H, 2.60; N, 15.03.

Synthesis of Os5. [$(NH_4)_2OsCl_6$] (62 mg, 0.14 mmol) and **14** (90 mg, 0.29 mmol) were combined in ethylene glycol (8 mL) and heated to reflux for 7 h. The reaction mixture was cooled to RT and treated with an aqueous solution (8 mL) of NH_4PF_6 (112 mg, 0.69 mmol). The resulting precipitate was collected by filtration, washed with H_2O, followed by Et_2O, and dried in vacuo. The solids were subsequently redissolved in MeCN (12 mL), refrigerated for 5 h, and then passed quickly through a short (2 cm) Celite pad. The addition of excess Et_2O to the filtrate reprecipitated a dark-green powder, which was purified further by column chromatography [Al_2O_3, 1:1:10 (v/v/v) H_2O/saturated aqueous KNO_3/MeCN]. Subsequent counterion metathesis furnished the desired complex as dark-green solids. Yield: 93 mg, 60%. ^{1}H NMR (MeCN-d_3, 400 MHz): δ 5.35 (s, 4H), 7.14 (d, J = 7.1 Hz, 4 H), 7.28−7.40 (m, 8H), 7.98 (t, J = 8.2 Hz, 2H), 8.11 (d, J = 3.3 Hz, 2H), 8.42 (d, J = 8.0 Hz, 2H), 8.58 (s, 2H), 8.72 (d, J = 8.1 Hz, 2H), 9.50 (d, J = 0.5 Hz, 2H). ^{13}C NMR (MeCN-d_3, 101 MHz): δ 56.60, 121.83, 121.99, 127.54, 129.42, 130.02, 130.09, 133.83, 138.28, 145.88, 147.53, 149.78, 151.32, 151.75, 155.66, 156.93. HRMS (ESI). Calcd for $[C_{36}H_{28}N_{12}Os]^{2+}$ (M^{2+}): m/z 410.1082. Found: m/z 410.1104. Calcd for $[C_{36}H_{28}N_{12}PF_6Os]^+$ (M^+): m/z 965.1817. Found: m/z 965.1825. Anal. Calcd for $C_{36}H_{28}N_{12}OsP_2F_{12}$: C, 38.99; H, 2.55; N, 15.16. Found: C, 38.80; H, 2.46; N, 15.04.

Synthesis of Os6. [$(NH_4)_2OsCl_6$] (77 mg, 0.17 mmol) and **17** (114 mg, 0.36 mmol) were combined in ethylene glycol (10 mL) and

DOI: 10.1021/acs.inorgchem.9b00915
Inorg. Chem. XXXX, XXX, XXX−XXX

heated to reflux for 7 h. The reaction mixture was cooled to RT and treated with an aqueous solution (10 mL) of NH_4PF_6 (146 mg, 0.89 mmol). The resulting precipitate was collected by filtration, washed with H_2O, followed by Et_2O, and dried in vacuo. Purification was carried out by column chromatography [SiO_2, 0.06:1:1:10 (v/v/v/v) Et_3N/H_2O/saturated aqueous KNO_3/MeCN], which, after counter-ion metathesis, afforded the product as a dark-green solid. Yield: 58 mg, 30%. ^{1}H NMR (MeCN-d_3, 400 MHz): δ 5.36 (s, 4H), 7.16 (d, J = 6.9 Hz, 4H), 7.29−7.40 (m, 6H), 7.45 (d, J = 3.2 Hz, 2H), 8.21 (d, J = 3.3 Hz, 2H), 8.73 (s, 2H), 9.46 (s, 2H), 9.69 (s, 2H), 9.81 (s, 2H). ^{13}C NMR (MeCN-d_3, 101 MHz): δ 56.85, 128.08, 129.58, 130.05, 130.19, 133.54, 142.36, 142.79, 145.12, 146.30, 148.67, 148.94, 149.50, 150.02, 154.38. HRMS (ESI). Calcd for $[C_{34}H_{26}N_{14}Os]^{2+}$ (M^{2+}): m/z 411.1034. Found: m/z 411.1044. Anal. Calcd for $C_{34}H_{26}N_{14}Os\ P_2F_{12}$: C, 36.76; H, 2.36; N, 17.65. Found: C, 36.89; H, 2.44; N, 17.83.

Computational Details. The ground-state geometries of the complexes were optimized in the gas phase at the B3LYP level of theory[64] using the Stuttgart−Dresden relativistic small-core effective core potential[65] and basis set for the osmium atom and 6-311G* basis sets[66] for all other atoms using the *NWChem* software package.[67] Molecular orbital energies and isosurface plots were then calculated in single-point calculations at the same level of theory using the SMD solvation model (MeCN).[68] HOMO and LUMO plots were produced using the *Gabedit*[69] viewer software. Time-dependent DFT calculations were also carried out including the solvation model, with the first 50 singlet and 10 triplet roots determined.

■ ASSOCIATED CONTENT

Supporting Information

The Supporting Information is available free of charge on the ACS Publications website at DOI: 10.1021/acs.inorgchem.9b00915.

NMR spectroscopy and mass spectrometry characterization data, additional electrochemical data, low-temperature (77 K) photoluminescence spectra, optimized geometry coordinates for **Os1**−**Os7**, and calculated UV−visible absorption spectra for **Os1**−**Os6** (PDF)

■ AUTHOR INFORMATION

Corresponding Authors

*E-mail: p.scattergood@hud.ac.uk.
*E-mail: p.i.elliott@hud.ac.uk.

ORCID

Paul A. Scattergood: 0000-0001-9070-5933
Paul I. P. Elliott: 0000-0003-1570-3289

Notes

The authors declare no competing financial interest.

■ ACKNOWLEDGMENTS

The authors thank the University of Huddersfield (PIPE and PAS) and the State of Libya (SAEO) for supporting this work. Via our membership of the U.K.'s HEC Materials Chemistry Consortium, which is funded by EPSRC (Grants EP/L000202 and EP/R029431), this work used the ARCHER U.K. National Supercomputing Service (http://www.archer.ac.uk). We acknowledge Orlando De Azevedo for useful synthetic discussions and also thank Stephen Boyer at London Metropolitan University for carrying out elemental microanalysis.

■ REFERENCES

(1) Xiang, H.; Cheng, J.; Ma, X.; Zhou, X.; Chruma, J. J. Near-infrared phosphorescence: materials and applications. *Chem. Soc. Rev.* **2013**, *42*, 6128−6185.

(2) Zhang, J.; Zhou, L.; Al-Attar, H. A.; Shao, K.; Wang, L.; Zhu, D.; Su, Z.; Bryce, M. R.; Monkman, A. P. Efficient Light-Emitting Electrochemical Cells (LECs) Based on Ionic Iridium(III) Complexes with 1,3,4-Oxadiazole Ligands. *Adv. Funct. Mater.* **2013**, *23*, 4667−4677.

(3) Kessler, F.; Costa, R. D.; Di Censo, D.; Scopelliti, R.; Orti, E.; Bolink, H. J.; Meier, S.; Sarfert, W.; Gratzel, M.; Nazeeruddin, M. K.; Baranoff, E. Near-UV to red-emitting charged bis-cyclometallated iridium(III) complexes for light-emitting electrochemical cells. *Dalton Trans.* **2012**, *41*, 180−191.

(4) Tamayo, A. B.; Garon, S.; Sajoto, T.; Djurovich, P. I.; Tsyba, I. M.; Bau, R.; Thompson, M. E. Cationic Bis-cyclometalated Iridium(III) Diimine Complexes and Their Use in Efficient Blue, Green, and Red Electroluminescent Devices. *Inorg. Chem.* **2005**, *44*, 8723−8732.

(5) Rudmann, H.; Shimada, S.; Rubner, M. F. Solid-State Light-Emitting Devices Based on the Tris-Chelated Ruthenium(II) Complex. 4. High-Efficiency Light-Emitting Devices Based on Derivatives of the Tris(2,2′-bipyridyl) Ruthenium(II) Complex. *J. Am. Chem. Soc.* **2002**, *124*, 4918−4921.

(6) Ertl, C. D.; Momblona, C.; Pertegás, A.; Junquera-Hernández, J. M.; La-Placa, M.-G.; Prescimone, A.; Ortí, E.; Housecroft, C. E.; Constable, E. C.; Bolink, H. J. Highly Stable Red-Light-Emitting Electrochemical Cells. *J. Am. Chem. Soc.* **2017**, *139*, 3237−3248.

(7) Ross, D. A. W.; Scattergood, P. A.; Babaei, A.; Pertegas, A.; Bolink, H. J.; Elliott, P. I. P. Luminescent osmium(II) bi-1,2,3-triazol-4-yl complexes: photophysical characterisation and application in light-emitting electrochemical cells. *Dalton Trans.* **2016**, *45*, 7748−7757.

(8) Bernhard, S.; Gao, X.; Malliaras, G. G.; Abruña, H. D. Efficient Electroluminescent Devices Based on a Chelated Osmium(II) Complex. *Adv. Mater.* **2002**, *14*, 433−436.

(9) Borek, C.; Hanson, K.; Djurovich, P. I.; Thompson, M. E.; Aznavour, K.; Bau, R.; Sun, Y.; Forrest, S. R.; Brooks, J.; Michalski, L.; Brown, J. Highly Efficient, Near-Infrared Electrophosphorescence from a Pt−Metalloporphyrin Complex. *Angew. Chem., Int. Ed.* **2007**, *46*, 1109−1112.

(10) Tuong Ly, K.; Chen-Cheng, R.-W.; Lin, H.-W.; Shiau, Y.-J.; Liu, S.-H.; Chou, P.-T.; Tsao, C.-S.; Huang, Y.-C.; Chi, Y. Near-infrared organic light-emitting diodes with very high external quantum efficiency and radiance. *Nat. Photonics* **2017**, *11*, 63.

(11) Lee, T.-C.; Hung, J.-Y.; Chi, Y.; Cheng, Y.-M.; Lee, G.-H.; Chou, P.-T.; Chen, C.-C.; Chang, C.-H.; Wu, C.-C. Rational Design of Charge-Neutral, Near-Infrared-Emitting Osmium(II) Complexes and OLED Fabrication. *Adv. Funct. Mater.* **2009**, *19*, 2639−2647.

(12) Liao, J.-L.; Chi, Y.; Yeh, C.-C.; Kao, H.-C.; Chang, C.-H.; Fox, M. A.; Low, P. J.; Lee, G.-H. Near infrared-emitting tris-bidentate Os(II) phosphors: control of excited state characteristics and fabrication of OLEDs. *J. Mater. Chem. C* **2015**, *3*, 4910−4920.

(13) Liao, J.-L.; Chi, Y.; Liu, S.-H.; Lee, G.-H.; Chou, P.-T.; Huang, H.-X.; Su, Y.-D.; Chang, C.-H.; Lin, J.-S.; Tseng, M.-R. Os(II) Phosphors with Near-Infrared Emission Induced by Ligand-to-Ligand Charge Transfer Transition. *Inorg. Chem.* **2014**, *53*, 9366−9374.

(14) Nishikitani, Y.; Cho, T.; Uchida, S.; Nishimura, S.; Oyaizu, K.; Nishide, H. Polymer-Based White-Light-Emitting Electrochemical Cells with Very High Color-Rendering Index Based on Blue-Green Fluorescent Polyfluorenes and Red-Phosphorescent Iridium Complexes. *ChemPlusChem* **2018**, *83*, 463−469.

(15) Sun, Y.; Forrest, S. R. High-efficiency white organic light emiting devices with three separate phosphorescent emisison layers. *Appl. Phys. Lett.* **2007**, *91*, 263503.

(16) Ikawa, S.; Yagi, S.; Maeda, T.; Nakazumi, H.; Sakurai, Y. White polymer light-emitting diodes co-doped with three phosphorescent iridium(III) complexes aimed at improvement of color rendering properties. *J. Lumin.* **2014**, *155*, 368−373.

DOI: 10.1021/acs.inorgchem.9b00915
Inorg. Chem. XXXX, XXX, XXX−XXX

(17) Zeng, Q.; Li, F.; Guo, T.; Shan, G.; Su, Z. Synthesis of red-emitting cationic Ir (III) complex and its application in white light-emitting electrochemical cells. *Org. Electron.* **2017**, *42*, 303−308.
(18) He, L.; Qiao, J.; Duan, L.; Dong, G.; Zhang, D.; Wang, L.; Qiu, Y. Toward Highly Efficient Solid-State White Light-Emitting Electrochemical Cells: Blue-Green to Red Emitting Cationic Iridium Complexes with Imidazole-Type Ancillary Ligands. *Adv. Funct. Mater.* **2009**, *19*, 2950−2960.
(19) Lemon, C. M.; Powers, D. C.; Brothers, P. J.; Nocera, D. G. Gold Corroles as Near-IR Phosphors for Oxygen Sensing. *Inorg. Chem.* **2017**, *56*, 10991−10997.
(20) Meng, T.-T.; Wang, H.; Zheng, Z.-B.; Wang, K.-Z. pH-Switchable "Off−On−Off" Near-Infrared Luminescence Based on a Dinuclear Ruthenium(II) Complex. *Inorg. Chem.* **2017**, *56*, 4775−4779.
(21) Pereira, N. A. M.; Laranjo, M.; Casalta-Lopes, J.; Serra, A. C.; Piñeiro, M.; Pina, J.; Seixas de Melo, J. S.; Senge, M. O.; Botelho, M. F.; Martelo, L.; Burrows, H. D.; Pinho e Melo, T. M. V. D. Platinum(II) Ring-Fused Chlorins as Near-Infrared Emitting Oxygen Sensors and Photodynamic Agents. *ACS Med. Chem. Lett.* **2017**, *8*, 310−315.
(22) Baggaley, E.; Weinstein, J. A.; Williams, J. A. G. Lighting the way to see inside the live cell with luminescent transition metal complexes. *Coord. Chem. Rev.* **2012**, *256*, 1762−1785.
(23) Coogan, M. P.; Fernandez-Moreira, V. Progress with, and prospects for, metal complexes in cell imaging. *Chem. Commun.* **2014**, *50*, 384−399.
(24) Zhao, Q.; Huang, C.; Li, F. Phosphorescent heavy-metal complexes for bioimaging. *Chem. Soc. Rev.* **2011**, *40*, 2508−2524.
(25) Liu, Y.; Zhang, P.; Fang, X.; Wu, G.; Chen, S.; Zhang, Z.; Chao, H.; Tan, W.; Xu, L. Near-infrared emitting iridium(III) complexes for mitochondrial imaging in living cells. *Dalton Trans.* **2017**, *46*, 4777−4785.
(26) Hagfeldt, A.; Boschloo, G.; Sun, L.; Kloo, L.; Pettersson, H. Dye-Sensitized Solar Cells. *Chem. Rev.* **2010**, *110*, 6595−6663.
(27) Numata, Y.; Singh, S. P.; Islam, A.; Iwamura, M.; Imai, A.; Nozaki, K.; Han, L. Enhanced Light-Harvesting Capability of a Panchromatic Ru(II) Sensitizer Based on π-Extended Terpyridine with a 4-Methylstylryl Group for Dye-Sensitized Solar Cells. *Adv. Funct. Mater.* **2013**, *23*, 1817−1823.
(28) Gong, J.; Sumathy, K.; Qiao, Q.; Zhou, Z. Review on dye-sensitized solar cells (DSSCs): Advanced techniques and research trends. *Renewable Sustainable Energy Rev.* **2017**, *68*, 234−246.
(29) Balzani, V.; Ceroni, P.; Juris, A. *Photochemistry and Photophysics: Concepts, Research, Applications*; Wiley-VCH, 2014.
(30) Ito, A.; Knight, T. E.; Stewart, D. J.; Brennaman, M. K.; Meyer, T. J. Rigid Medium Effects on Photophysical Properties of MLCT Excited States of Polypyridyl Os(II) Complexes in Polymerized Poly(ethylene glycol)dimethacrylate Monoliths. *J. Phys. Chem. A* **2014**, *118*, 10326−10332.
(31) Chen, K.; Cheng, Y.-M.; Chi, Y.; Ho, M.-L.; Lai, C.-H.; Chou, P.-T.; Peng, S.-M.; Lee, G.-H. Osmium Complexes with Tridentate 6-Pyrazol-3-yl 2,2′-Bipyridine Ligands: Coarse Tuning of Phosphorescence from the Red to the Near-Infrared Region. *Chem. - Asian J.* **2007**, *2*, 155−163.
(32) Byrne, A.; Dolan, C.; Moriarty, R. D.; Martin, A.; Neugebauer, U.; Forster, R. J.; Davies, A.; Volkov, Y.; Keyes, T. E. Osmium(II) polypyridyl polyarginine conjugate as a probe for live cell imaging; a comparison of uptake, localization and cytotoxicity with its ruthenium(II) analogue. *Dalton Trans.* **2015**, *44*, 14323−14332.
(33) Zhang, P.; Wang, Y.; Qiu, K.; Zhao, Z.; Hu, R.; He, C.; Zhang, Q.; Chao, H. A NIR phosphorescent osmium(II) complex as a lysosome tracking reagent and photodynamic therapeutic agent. *Chem. Commun.* **2017**, *53*, 12341−12344.
(34) Ge, C.; Huang, H.; Wang, Y.; Zhao, H.; Zhang, P.; Zhang, Q. Near-Infrared Luminescent Osmium(II) Complexes with an Intrinsic RNA-Targeting Capability for Nucleolus Imaging in Living Cells. *ACS Appl. Bio Mater.* **2018**, *1*, 1587−1593.
(35) Omar, S. A. E.; Scattergood, P. A.; McKenzie, L. K.; Jones, C.; Patmore, N. J.; Meijer, A. J. H. M.; Weinstein, J. A.; Rice, C. R.; Bryant, H. E.; Elliott, P. I. P. Photophysical and Cellular Imaging Studies of Brightly Luminescent Osmium(II) Pyridyltriazole Complexes. *Inorg. Chem.* **2018**, *57*, 13201−13212.
(36) Omar, S. A. E.; Scattergood, P. A.; McKenzie, L. K.; Bryant, H. E.; Weinstein, J. A.; Elliott, P. I. P. Towards Water Soluble Mitochondria-Targeting Theranostic Osmium(II) Triazole-Based Complexes. *Molecules* **2016**, *21*, 1382.
(37) Zhao, X.; Li, M.; Sun, W.; Fan, J.; Du, J.; Peng, X. An estrogen receptor targeted ruthenium complex as a two-photon photodynamic therapy agent for breast cancer cells. *Chem. Commun.* **2018**, *54*, 7038−7041.
(38) Kershaw Cook, L. J.; Tuna, F.; Halcrow, M. A. Iron(II) and cobalt(II) complexes of tris-azinyl analogues of 2,2′:6′,2″-terpyridine. *Dalton Trans.* **2013**, *42*, 2254−2265.
(39) Rocha, R. C.; Shreve, A. P. Exploring the Localized-to-Delocalized Boundary in Mixed-Valence Systems Using Infrared Spectroelectrochemistry. *Inorg. Chem.* **2004**, *43*, 2231−2233.
(40) Padilla, R.; Ruminski, R. R.; Meredith McGinley, V. A.; Williams, P. B. The syntheses and characterization of Os(II) and Ru(II)/Os(II) bimetallic complexes with dipyrido(2,3-a:3′,2′j)-phenazine (dpop′) and the bridging ligand 2,3,5,6-tetra(2-pyridyl)-pyrazine (tppz). *Polyhedron* **2012**, *33*, 158−165.
(41) Knoll, J. D.; Arachchige, S. M.; Wang, G.; Rangan, K.; Miao, R.; Higgins, S. L. H.; Okyere, B.; Zhao, M.; Croasdale, P.; Magruder, K.; Sinclair, B.; Wall, C.; Brewer, K. J. Electrochemical, Spectroscopic, and Photophysical Properties of Structurally Diverse Polyazine-Bridged Ru(II),Pt(II) and Os(II),Ru(II),Pt(II) Supramolecular Motifs. *Inorg. Chem.* **2011**, *50*, 8850−8860.
(42) Brauns, E.; Jones, S. W.; Clark, J. A.; Molnar, S. M.; Kawanishi, Y.; Brewer, K. J. Electrochemical, Spectroscopic, and Spectroelectrochemical Properties of Synthetically Useful Supramolecular Light Absorbers with Mixed Polyazine Bridging Ligands. *Inorg. Chem.* **1997**, *36*, 2861−2867.
(43) Zigler, D. F.; Mongelli, M. T.; Jeletic, M.; Brewer, K. J. A trimetallic supramolecular complex of osmium(II) and rhodium(III) displaying MLCT transitions in the near-IR. *Inorg. Chem. Commun.* **2007**, *10*, 295−298.
(44) Baudin, H. B.; Davidsson, J.; Serroni, S.; Juris, A.; Balzani, V.; Campagna, S.; Hammarström, L. Ultrafast Energy Transfer in Binuclear Ruthenium−Osmium Complexes as Models for Light-harvesting Antennas. *J. Phys. Chem. A* **2002**, *106*, 4312−4319.
(45) Ruminski, R. R.; Zimmer, K. D. K.; Rita, K. A.; Knobbe, M. A.; Dean, C. Synthesis and characterization of Os(II)(dpop′) (dpop′=dipyrido(2,3-a;3′,2′-j)phenazine) complexes with 2,2′-bipyridine(bpy); 2,2′-bipyrimidine(bpm) and 2,3-bis(2-pyridyl)-pyrazine(dpp). *Inorg. Chim. Acta* **2009**, *362*, 1772−1780.
(46) Allampally, N. K.; Daniliuc, C.-G.; Strassert, C. A.; De Cola, L. Tuning the Structural and Photophysical Properties of Cationic Pt(II) Complexes Bearing Neutral Bis(triazolyl)pyridine Ligands. *Inorg. Chem.* **2015**, *54*, 1588−1596.
(47) Crowley, J. D.; Bandeen, P. H.; Hanton, L. R. A one pot multi-component CuAAC "click" approach to bidentate and tridentate pyridyl-1,2,3-triazole ligands: Synthesis, X-ray structures and copper-(II) and silver(I) complexes. *Polyhedron* **2010**, *29*, 70−83.
(48) Bronner, C.; Wenger, O. S. Long-range proton-coupled electron transfer in phenol-Ru(2,2′-bipyrazine)$_3^{2+}$ dyads. *Phys. Chem. Chem. Phys.* **2014**, *16*, 3617−3622.
(49) Darabantu, M.; Boully, L.; Turck, A.; Plé, N. Synthesis of new polyaza heterocycles. Part 42: Diazines. *Tetrahedron* **2005**, *61*, 2897−2905.
(50) Dick, G. R.; Knapp, D. M.; Gillis, E. P.; Burke, M. D. General Method for Synthesis of 2-Heterocyclic N-Methyliminodiacetic Acid Boronates. *Org. Lett.* **2010**, *12*, 2314−2317.
(51) Knapp, D. M.; Gillis, E. P.; Burke, M. D. A General Solution for Unstable Boronic Acids: Slow-Release Cross-Coupling from Air-Stable MIDA Boronates. *J. Am. Chem. Soc.* **2009**, *131*, 6961−6963.

DOI: 10.1021/acs.inorgchem.9b00915
Inorg. Chem. XXXX, XXX, XXX−XXX

(52) Felix, F.; Ferguson, J.; Güdel, H. U.; Ludi, A. Electronic spectra of $M(bipy)_3^{2+}$ complexions (M = Fe, Ru and Os). *Chem. Phys. Lett.* **1979**, *62*, 153−157.
(53) Suzuki, K.; Kobayashi, A.; Kaneko, S.; Takehira, K.; Yoshihara, T.; Ishida, H.; Shiina, Y.; Oishi, S.; Tobita, S. Reevaluation of absolute luminescence quantum yields of standard solutions using a spectrometer with an integrating sphere and a back-thinned CCD detector. *Phys. Chem. Chem. Phys.* **2009**, *11*, 9850−9860.
(54) Kober, E. M.; Caspar, J. V.; Lumpkin, R. S.; Meyer, T. J. Application of the energy gap law to excited-state decay of osmium(II)-polypyridine complexes: calculation of relative non-radiative decay rates from emission spectral profiles. *J. Phys. Chem.* **1986**, *90*, 3722−3734.
(55) Caspar, J. V.; Kober, E. M.; Sullivan, B. P.; Meyer, T. J. Application of the energy gap law to the decay of charge-transfer excited states. *J. Am. Chem. Soc.* **1982**, *104*, 630−632.
(56) Chen, Y.-L.; Lee, S.-W.; Chi, Y.; Hwang, K.-C.; Kumar, S. B.; Hu, Y.-H.; Cheng, Y.-M.; Chou, P.-T.; Peng, S.-M.; Lee, G.-H.; Yeh, S.-J.; Chen, C.-T. Synthesis, Characterization, and Photophysical Properties of Os(II) Diimine Complexes $[Os(N^\wedge N)(CO)_2I_2]$ (N^N = Bipyridine, Phenanthroline, and Pyridyl Benzoxazole). *Inorg. Chem.* **2005**, *44*, 4287−4294.
(57) Sauvage, J. P.; Collin, J. P.; Chambron, J. C.; Guillerez, S.; Coudret, C.; Balzani, V.; Barigelletti, F.; De Cola, L.; Flamigni, L. Ruthenium(II) and Osmium(II) Bis(terpyridine) Complexes in Covalently-Linked Multicomponent Systems: Synthesis, Electrochemical Behavior, Absorption Spectra, and Photochemical and Photophysical Properties. *Chem. Rev.* **1994**, *94*, 993−1019.
(58) Rillema, D. P.; Allen, G.; Meyer, T. J.; Conrad, D. Redox properties of ruthenium(II) tris chelate complexes containing the ligands 2,2′-bipyrazine, 2,2′-bipyridine, and 2,2′-bipyrimidine. *Inorg. Chem.* **1983**, *22*, 1617−1622.
(59) Maruszewski, K.; Strommen, D. P.; Kincaid, J. R. Zeolite-entrapped ruthenium(II) complexes with bipyridine and related ligands. Elimination of ligand-field-state deactivation and increase in ^{3}MLCT state lifetimes. *J. Am. Chem. Soc.* **1993**, *115*, 8345−8350.
(60) Lee, C.-W.; Ouyang, J.; Bard, A. J. Electrogenerated chemiluminescence: Part 51. The tris(2,2′-bipyrazine)osmium(II) system. *J. Electroanal. Chem. Interfacial Electrochem.* **1988**, *244*, 319−324.
(61) Campbell-Verduyn, L. S.; Mirfeizi, L.; Dierckx, R. A.; Elsinga, P. H.; Feringa, B. L. Phosphoramidite accelerated copper(i)-catalyzed [3 + 2] cycloadditions of azides and alkynes. *Chem. Commun.* **2009**, 2139−2141.
(62) Hoang, T. N. Y.; Humbert-Droz, M.; Dutronc, T.; Guénée, L.; Besnard, C.; Piguet, C. A Polyaromatic Terdentate Binding Unit with Fused 5,6-Membered Chelates for Complexing s-, p-, d-, and f-Block Cations. *Inorg. Chem.* **2013**, *52*, 5570−5580.
(63) Wang, S.; Cuesta-Seijo, J. A.; Lafont, D.; Palcic, M. M.; Vidal, S. Design of Glycosyltransferase Inhibitors: Pyridine as a Pyrophosphate Surrogate. *Chem. - Eur. J.* **2013**, *19*, 15346−15357.
(64) Stephens, P. J.; Devlin, F. J.; Chabalowski, C. F.; Frisch, M. J. Ab Initio Calculation of Vibrational Absorption and Circular Dichroism Spectra Using Density Functional Force Fields. *J. Phys. Chem.* **1994**, *98*, 11623−11627.
(65) Andrae, D.; Häußermann, U.; Dolg, M.; Stoll, H.; Preuß, H. Energy-adjustedab initio pseudopotentials for the second and third row transition elements. *Theor Chim. Acta* **1990**, *77*, 123−141.
(66) Krishnan, R.; Binkley, J. S.; Seeger, R.; Pople, J. A. Self-consistent molecular orbital methods. XX. A basis set for correlated wave functions. *J. Chem. Phys.* **1980**, *72*, 650−654.
(67) Valiev, M.; Bylaska, E. J.; Govind, N.; Kowalski, K.; Straatsma, T. P.; Van Dam, H. J. J.; Wang, D.; Nieplocha, J.; Apra, E.; Windus, T. L.; de Jong, W. A. NWChem: A comprehensive and scalable open-source solution for large scale molecular simulations. *Comput. Phys. Commun.* **2010**, *181*, 1477−1489.
(68) Marenich, A. V.; Cramer, C. J.; Truhlar, D. G. Universal Solvation Model Based on Solute Electron Density and on a Continuum Model of the Solvent Defined by the Bulk Dielectric Constant and Atomic Surface Tensions. *J. Phys. Chem. B* **2009**, *113*, 6378−6396.
(69) Allouche, A.-R. Gabedit—A graphical user interface for computational chemistry softwares. *J. Comput. Chem.* **2011**, *32*, 174−182.

DOI: 10.1021/acs.inorgchem.9b00915
Inorg. Chem. XXXX, XXX, XXX−XXX